Journal of Marine Research, 66, 835–872, 2008

Observations of coastal upwelling off Uruguay downshelf of the Plata estuary, South America

by Felipe Pimenta[1,2], Richard W. Garvine[1,3] and Andreas Münchow[1]

ABSTRACT

We analyze hydrographic and current observations of an upwelling center off eastern South America on the Uruguayan coast (~35S) and downshelf from the Rio de la Plata estuary. Our observations show that the buoyancy-driven subtidal alongshore circulation is modulated by winds. During the winter, strong upwelling-favorable local winds forced the Rio de la Plata buoyant plume poleward. In the summer, the plume detached from the coast with warm and saline subtropical waters intruding from the north. These waters bounded the upwelling of cold waters in the nearshore area off Uruguay. A shallow submarine canyon cutting obliquely across the shelf facilitates the advection of cold waters into the coastal upwelling domain. An upwelling jet was detected off Uruguay for summer conditions, while for winter the plume configuration generated strong horizontal shear of along-shelf currents. Cross-shelf circulation was dependent on the coastal stratification. Under low stratification (summer) a two-layer circulation developed, with thick surface and bottom mixed layers flowing in opposite directions. High stratification levels (winter) modified this pattern by allowing circulation along a thick stratified interior.

The existence of upwelling was linked to the history of wind events and shelf stratification. During the winter, downwelling winds frequently restore the plume, so the upwelling efficiency is very low. In the summer, downwelling events are less frequent and intense, so that the cumulative effect of upwelling events act to export the Plata freshwaters offshore. The reduction of inner-shelf stratification increases the likelihood of a full upwelling to the surface. Analysis of the wind-induced Ekman transport suggests that the Uruguay upwelling system reflects a seasonal wind pattern modulated by significant interannual variability.

1. Introduction

Coastal upwelling is an important oceanic process occurring in many continental shelves and the basic mechanism of this phenomenon is well described in the literature. Alongshore winds act on the ocean to move its surface waters away from the coast, bringing deeper nutrient enriched cold waters to the surface (Smith, 1994; Hill *et al.,* 1998). As a result, these regions are characterized by high biological productivity and attendant impact on world's fisheries (Bakun, 1996; Summerhayes *et al.,* 1994).

1. College of Marine and Earth Studies, University of Delaware, Newark, Delaware, 19716, U.S.A.
2. Corresponding author. ***email: felipe@udel.edu***
3. Deceased.

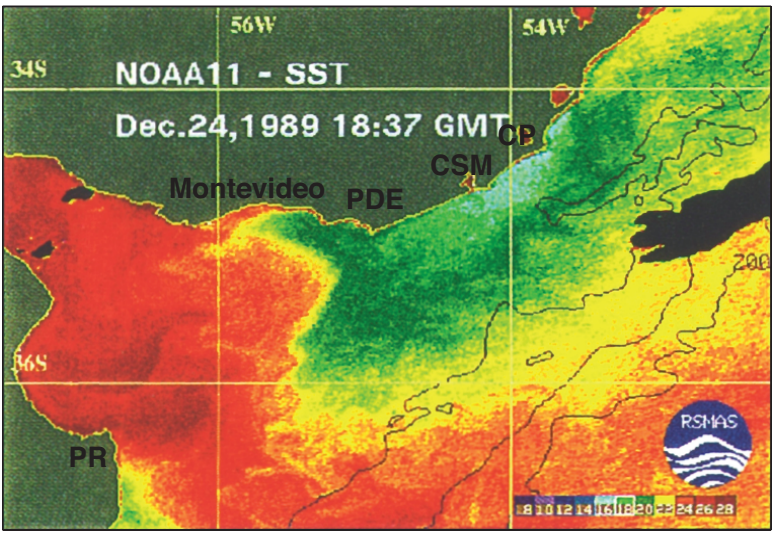

Figure 1. Sea-surface temperature reproduced from Framiñan *et al.* (1999) for December 24th 1989 depicting the upwelling of cold waters off the Uruguayan coast. Red colors indicate warmer (T ~ 26°C) and blue-greenish colors colder (T ~ 16–20°C) temperatures. The labels indicate Punta del Este (PDE), Cape Santa Maria (CSM), Cape Polonio (CP) and Punta Rasa (PR). Image reproduced with permission of Springer Verlag.

The divergence of the surface flow in upwelling regions is often expressed in terms of wind-driven Ekman transport, which agrees well with that measured directly from current meters (Lentz, 1992). The complete upwelling circulation, however, depend on the details of wind forcing, topography, ambient currents, coastline configuration, as well as the vertical and horizontal stratification of the continental shelves.

In this study we focus on observations of an upwelling center off Uruguay in South America (~35S). Framiñan *et al.* (1999) first described aspects of this upwelling system using AVHRR sea-surface temperature imagery (Fig. 1). The authors describe the occurrence of coastal upwelling from the surface cold-water signature (T ~ 18°C) for the summer of 1989. The image depicts the outcropping of bottom waters to the surface, where the upwelling center occupy the stretch of coast from Cape Polonio (CP) past Punta del Este (PDE) (Fig. 1).

The upwelling occurs in a complex physical setting (Fig. 2a) as Uruguay is located to the north of the Rio de la Plata estuary, a shallow (~15 m) funnel-shaped estuarine system. The estuarine external and internal Kelvin numbers are $K_e \approx 1.4$ and $K_i > 12$, respectively at its mouth, which is about 230 km wide. These were calculated from $K_e = b/R_{de}$ and $K_i = b/R_{di}$, where b is the estuary breadth and $R_{de} = \sqrt{gh}/f$ is the external; and $R_{di} = \sqrt{g'h}/f$ the internal Rossby radius of deformation ($g' = g\Delta\rho/\rho_o$ is the reduced gravity and f is the Coriolis parameter). The importance of rotation in the barotropic flow is indicated by $K_e = O(1)$.

The shelf has a weak tidal regime and is too short for resonance to occur. The semi-diurnal resonance parameter (Clarke and Battisti, 1981) is $\mu L_s \sim 0.17$ at 35S ($\mu = (\omega^2 - f^2)/g\alpha$, where α = shelf bottom slope, ω = tidal frequency and L_s is the shelf width). This contrasts with the Argentinean shelf where $\mu L_s \sim 1.23$ and the tides dominate the dynamics southward of 39S (Palma *et al.,* 2004). The bottom has a mild slope ($\alpha \sim 10^{-3}$) and relatively broad extension (~160 km), but is marked by the presence of a narrow canyon, which cuts the region obliquely and connects deeper reaches of the shelf (~70 m) to the nearshore area between Punta del Este and Cape Polonio (Fig. 2a).

Offshore of the shelfbreak two major western boundary currents converge. The relatively warm and salty tropical waters of Brazil Current (BC) flow southward along the continental slope as the western part of the Subtropical Gyre (Stramma and England, 1999; Silveira *et al.,* 2000). The relatively cold and fresh Malvinas (Falkland) Current (MC) flows northward along the Argentinean shelfbreak, originating from the Antarctic Circumpolar Current. These currents collide in deep waters and flow eastward around 37.5S in the Brazil-Malvinas Confluence (BMC), a region characterized by strong meanders and eddy activity (Olson *et al.,* 1988; Vivier and Provost, 1999) (Fig. 2a). Despite the broad continental shelf, these oceanic currents extend their influence over shallower waters in the form a Subtropical Shelf Front (STSF) which divides shelf waters of subtropical properties (Subtropical Shelf Water, STSW) from waters of diluted subantarctic origin (Subantarctic Shelf Water, SASW) (Fig. 2b) (Piola *et al.,* 2000, 2008).

The Uruguayan shelf receives about Q~23000 $m^3\ s^{-1}$ of freshwater from the Rio de la Plata in the form a large-scale plume, which exits the estuary and turns downshelf[4], often extending to low latitudes in southern Brazil (Emilson, 1960; Miranda, 1972; Castello and Möller, 1977; Guerrero *et al.,* 1997; Moller *et al.,* 2008). The density field set up by the riverine waters drives a northward buoyancy-driven flow (Pereira, 1989; Soares *et al.,* 2001; Zavialov *et al.,* 2002). The plume experiences large seasonal changes. Its shorter along-shelf extension is observed in the summer when its northernmost surface signal reaches 32S (Fig. 2a). During the austral winter, a band of low salinity extends ~960 km from the mouth of the estuary to Cape Santa Marta in southern Brazil (28S) (Piola *et al.,* 2000; Möller *et al.,* 2008) (Fig. 2a). This low salinity front has been postulated to be a near-permanent feature of the nearshore waters off Uruguay from the analysis of historical observations (Bakun, 1996, Fig. 10.6; Acha *et al.,* 2004, Fig. 2, Piola *et al.* 2000, Fig. 3). This assumption, however, conflicts with the occurrence of the upwelling temperature front that we will report here.

Previous studies considered the effects of remote sources of buoyancy (Garvine, 2004; Huyer *et al.,* 2005) and deep shelfbreak canyons (e.g. Freeland and Denman, 1982; Hickey, 1997) on the dynamics of upwelling. For deep shelf canyons, the along-shelf flow usually

4. The term *downshelf* refers to the direction of Kelvin wave propagation; regarded as northward (equatorward) for the Uruguay shelf. The term *upshelf* is used to refer to the opposite direction (i.e. southward or poleward).

dictates the fate of upwelling (Klinck, 1996; She and Klinck, 2000). In particular, the mechanism of exchange involves pressure gradients established across the canyon so that the upwelling flow can be interpreted as a geostrophic response to an ambient pressure field (Kämpf, 2006). Remote sources of buoyancy, on the other hand, modify the structure of

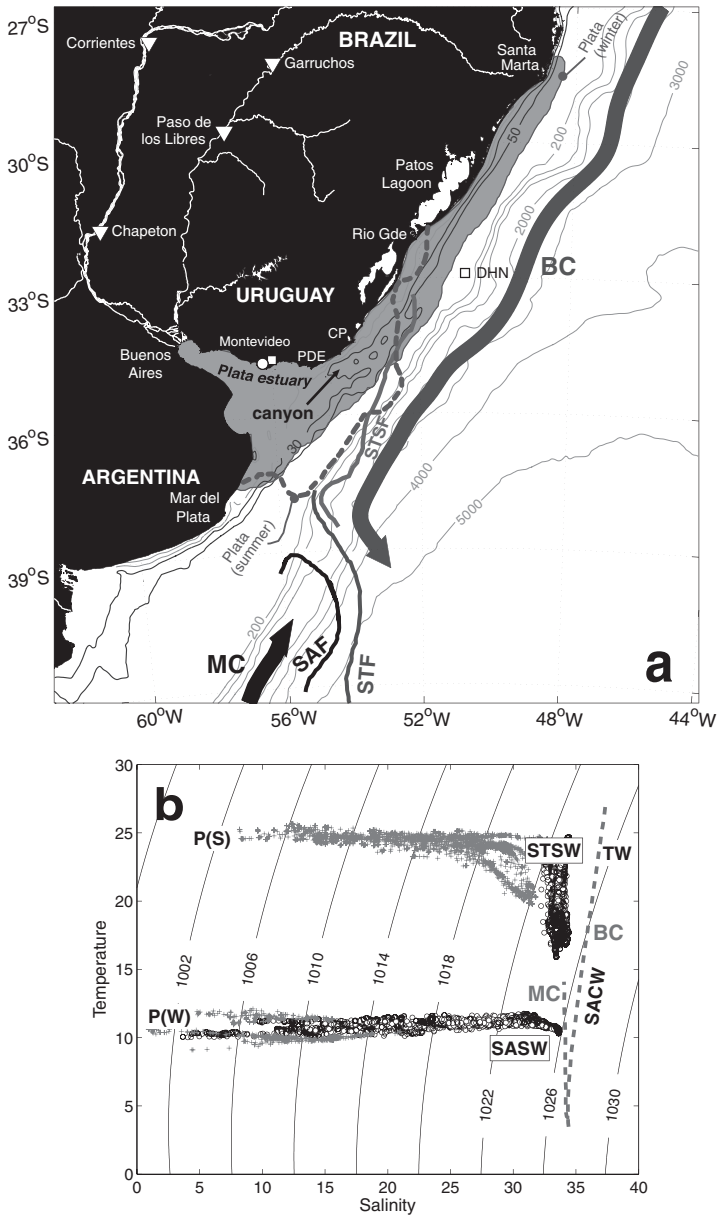

along-shelf and across-shelf circulation, episodically isolating the interior layers from the wind-induced turbulent mixing (Yankovsky *et al.,* 2000).

Off Uruguay the upwelling center differs as it is very close to the Rio de la Plata buoyancy source and to a shallow canyon that runs obliquely across the entire shelf. It is uncertain how the proximity to Plata estuary should affect the dynamics of the upwelling center or the Uruguay along-shelf circulation. Furthermore, it is unknown how the plume should respond to synoptic wind forcing. Should Plata behavior be similar to that known for other coastal plumes? Can the plume freshwaters inhibit the upwelling off Uruguay? What role does stratification play on across-shelf circulation? How important is the canyon to the occurrence of upwelling?

This study builds upon two ADCP and hydrographic ship surveys conducted in August of 1999 and January/February of 2000 to explore different aspects of the Uruguay shelf dynamics. Both cruises covered upwelling-favorable events, but different seasons and magnitudes of river discharge. Here we focus on the analysis of these observations, their upwelling frontal structures and the response of Plata plume to wind forcing.

2. Dataset

In the winter of 1999 and summer of 2000 a collaborative observational study, RioPla[5], was conducted off Uruguay and Argentina, surveying different regions of the Rio de la Plata estuary and its adjacent coastal currents. Fieldwork consisted of shipborne velocity and hydrographic sections that covered upshelf, central and downshelf areas of the estuary.

5. "Collaborative observational study of estuarine and coastal dynamics in the Rio de la Plata, South America. RioPla Project" (NSF International program, ref. OCE-9529806).

←

Figure 2. (a) Rio de la Plata estuary and relevant oceanographic and geomorphologic features of SE South America continental shelf. Brazil (BC) and Malvinas (MC) currents are shown schematically by thick arrows. Subtropical (STF) and Subantartic Fronts (SAF) indicate the oceanic confluence, as shown in Vivier and Provost (1999). The gray shade represents Plata plume winter position (S∼33 psu) as derived from historical data (Piola *et al.,* 2000). The summer position is shown by a dashed gray line. A continuous gray line indicates the Subtropical Shelf Front (STSF) position (Piola *et al.,* 2000). Depth contours are indicated and the thicker lines denote the 30- and 50-m isobaths, delimiting the Plata canyon. PDE and CP labels are Punta del Este and Cape Polonio. The wind station of Carrasco and the meteorological buoy (DHN) are shown by white squares. A bullet indicates the tidal gauge location in Montevideo. Stream-gauges for the Paraná (Corrientes and Chapetón) and Uruguay (Garruchos and Paso de los Libres) rivers are indicated by triangles. (b) Temperature-salinity diagram with density contours. Symbols indicate RioPla observations, with black circles indicating downshelf casts (along Uruguay coast) and gray crosses mid-estuary and upshelf profiles (along the Argentinean coast). Labels P(S) and P(W) stand for Plata summer and winter characteristics (Guerrero *et al.,* 1997). Other labels are SACW: South Atlantic Central Water, SASW: Subantartic Shelf Waters and STSW: Subtropical Shelf Waters (Stramma and England, 1999; Silveira *et al.,* 2000; Piola *et al.,* 2000).

We refer to Sepulveda *et al.* (2004) and Dragani *et al.* (2002) for works related to aspects of the circulation inside the estuary. Here we focus on the analysis of the winter and summer shelf surveys along the coast of Uruguay, conducted by the hydrographic ship *Comodoro Rivadavia* of the Argentinean Navy. Preliminary descriptions of this dataset are found in Münchow and Framiñan (2000, 2001) and Framiñan (2005).

A total of 13 long transects for winter (August, 15th to 20th, 1999) and 13 for summer (January 26th to February 2nd, 2000) were surveyed between Montevideo and Cape Polonio (Fig. 3a,b). Transects names were sequentially numbered from the estuary to the shelf, with the summer (winter) transects prefixed by a capital "S" (W). We designate repeated transects with an alphabetic suffix, e.g. S10a.

Most sections extended across the shelf from within 2 km off the coast to 35–70 km offshore, covering parts of the Oriental Channel and the Plata canyon (see Fig. 3a). The Oriental Channel is part of the ancient drowned river valley of the Rio de la Plata (Laborde and Nagy, 1999). The drowned valley or canyon is commonly referred to as "mud basin" (Pozos de Fango in Spanish). The canyon reaches 80-m depth offshore of Cape Santa Maria and its breadth varies from 5 to 20 km (Fig. 3c). Offshore of the depression, La Plata bank appear as another prominent topographic feature in the region, with depths shallower than 30 m. Specifically for the summer, an additional small-scale survey was conducted between Cape Santa Maria and Maldonado, covering nearly 50 km of coastline. Eight cross-shelf sections of about 15 km long were surveyed between the coast and the Plata canyon rim (Fig. 3b).

Velocity fields were sampled with a downward looking 307 kHz ADCP of RD Instruments mounted in a vehicle towed besides the ship at 3- to 4-m depth (Münchow *et al.,* 1995). Hydrographic profiles were measured by an Ocean Sensor OS200 and a Seabird SBE19 CTD. A total of 100 CTD casts were taken along the ADCP tracks in winter and nearly 132 in the summer. Underway measurements from another Seabird SBE19 installed inside the towed body provided pressure, temperature, and salinity along the ship's track for sound speed corrections and near-surface mapping of thermohaline fields.

Temperature and salinity data were processed with the software provided by the CTD manufacturers. Doppler velocities were sampled in beam coordinates and in bottom tracking mode at all times. Transects data were pre-screened for attitude (heading, pitch and roll) as well as for correlation, error velocity and percent good ($>$85%) of bottom track. GPS (Global Positioning System) was used for quality control avoiding data sampled during ship stoppage, accelerations, and sharp navigation turns. Water Doppler velocity components were post-screened for percent good pings and vertical velocity. The calibration of the ADCP compass followed Joyce (1989) and Münchow *et al.* (1995). Earth-velocity components were averaged for 25-point ensembles after calibration, resulting in a time step of 2 to 5 minutes between measurements. The upper 6 m of water column were not sampled, due to the depth of operation of the towed fish and the lower 6% of the water column was discarded to avoid acoustic side-lobe interference (RD Instruments, 1996). Tidal currents were extracted from the towed ADCP velocities by applying the

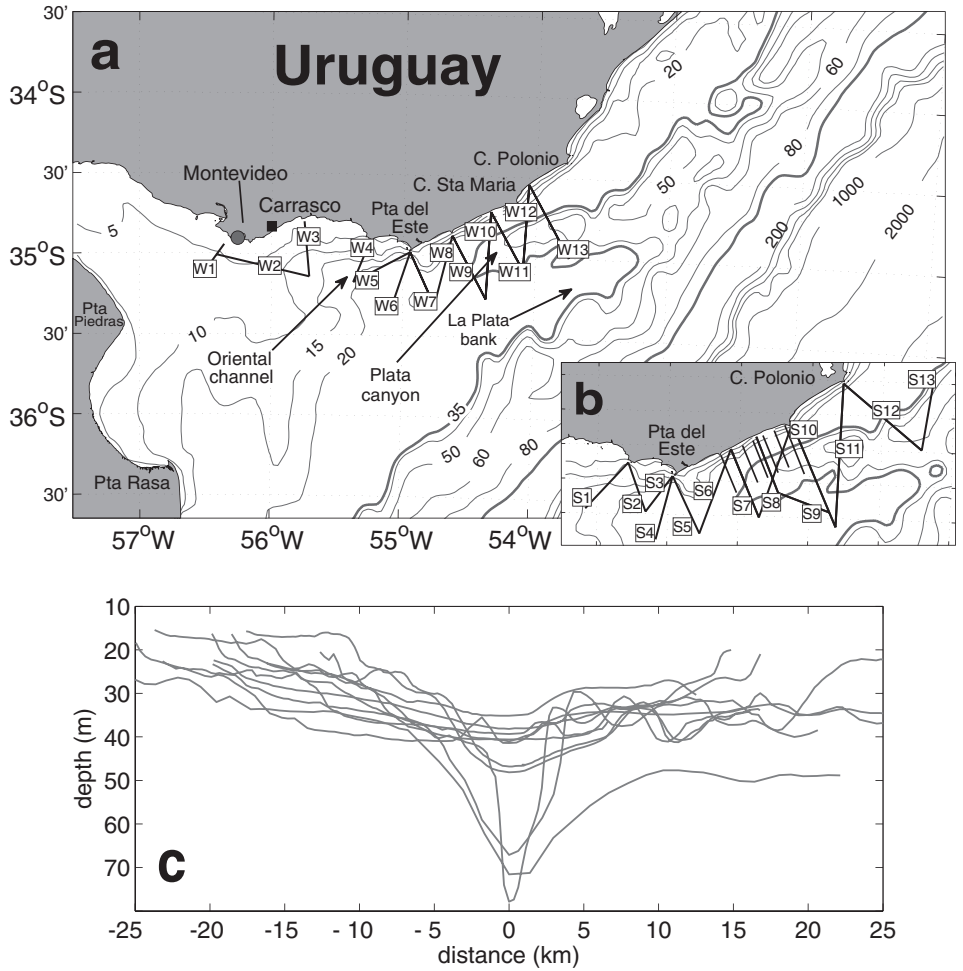

Figure 3. Map of the study area (a and b) and selected across-shelf bottom depths (c). Winter (August 15th to 20th, 1999) transect positions are displayed in (a) and summer (January 26th to February 2nd, 2000) transects in (b). Boxed labels indicate section names of major transects (straight lines). Thin lines on the insert map represent the summer small-scale survey. Bottom bathymetry covers the estuary and shelf, with a thicker line depicting the 35 and the 100-m isobaths. A square indicates Carrasco wind tower and a bullet the Montevideo tidal gauge location. Arrows indicate important geomorphologic features of Uruguay shelf: the Oriental channel, Plata canyon and La Plata bank. Bathymetric profiles in (c) are derived from the towed ADCP. Note that Plata canyon runs nearly parallel to Uruguay coastline and oblique to shelf slope. Its breadth varies from 5 to 20 km and its maximum depths, close to 80 m, are observed on the northern transects (e.g. S12 and W13).

method originally developed in Candela *et al.* (1992). The method is analogous to the classic harmonic analysis of tidal currents, but with allowance for amplitudes and phases that vary in space. The method employed uses biharmonic splines as radial base functions

to find the spatial variations of prescribed tidal constituents (Wang *et al.,* 2003; Wang, 2007). Here we analyzed for the semi-diurnal (M_2) and diurnal (O_1) tidal components, which are the dominant constituents in the region (Simionato *et al.,* 2005). Both winter and summer data were used in the least-squares method with a total coverage of nearly 9 days. Because the duration of cruises was relatively short we have not tried to resolve other individual harmonics. Therefore, the fit of our tidal currents lumps all semidiurnal energy to M_2 and diurnal to O_1 (Foreman and Freeland, 1991; Emery and Thomson, 1997). Four nodal positions were selected for the analysis, after a set of tests with synthetic tides. Tidal ellipses for M_2 were dominant and presented major axis generally oriented along the isobaths, with stronger currents for shallower regions and around the coastal headlands. Computed semidiurnal constituents from this analysis averaged 0.12 ms^{-1} semi-major amplitudes, compared to 0.08 ms^{-1} for the diurnal ellipses. Detided velocity fields were obtained by subtracting M_2 and O_1 predicted tidal currents from the of ADCP measurements.

River outflow was obtained from the Argentine Department of Hydrology stream-flow gauges (Fig. 2a). Discharge data from the Rio de la Plata Estuary was obtained by summing the series of Paraná and Uruguay rivers, respectively, measured at Chapetón (Station 3005; 31.65S, 60.28W) and Paso de los Libres (St. 3802; 29.72S, 57.08W). Measurements at Chapetón are located about 420 km upstream from the estuary head and include the contributions of the Paraná and Paraguay rivers (Berbery and Barros, 2002). Measurements at Paso de los Libres are situated ~530 km upstream of the estuary head. The temporal delay of the river discharge from these stations to the estuary head its unknown, so we estimated it from the flood propagation speed, as measured by different gauges positioned along these rivers to arrive at temporal lags between 6–9 days between upstream river gauging stations to the mouth of the estuary. The temporal lag was obtained from the maximum cross-correlation between upstream and downstream river stations. The upstream stations used were Corrientes (St. 3805, 27.58S, 58.70W) for Paraná and Garruchos (St. 3857, 28.18S, 55.64W) for the Uruguay river (Fig. 2a).

NCEP Reanalysis (Kalnay *et al.,* 1996) of sea-level pressure and surface winds as well as scatterometer data from the QuikSCAT satellite (JPL/PO.DAAC; Level 3b) were used to observe the spatial structure of the wind fields during the field operations. The QuikSCAT dataset we use covers a period from August 1999 to June 2007 at a resolution of 25 km. The temporal resolution of QuikSCAT depends on orbital patterns, but most times 2 observations are available per day. QuikSCAT was previously validated in comparisons to offshore meteorological buoys (Ebuchi *et al.,* 2002) and to coastal buoys observations that are less than 30 km from shoreline (Picket *et al.,* 2003). These studies found root mean square (rms) errors for wind speed between 1 m s^{-1} and 1.4 m s^{-1}. Wind direction rms difference was ~20° for higher wind speeds (>3 m s^{-1}).

High temporal resolution meteorological station data were measured from an anemometer tower over land and from a meteorological buoy maintained by the Brazilian Navy (Station DHN; 50.80W, 32.90S) (Fig. 2a). The buoy data time series (2001–2004) does not

cover the periods of our 1999–2000 surveys, however, it provided comparison data to the QuikSCAT scatterometer data. These two wind series correlate at R = 0.9 with an rms difference of 1 m s^{-1} and less than 30° for wind direction.

A longer wind series, which covered the period of our surveys, was provided by the meteorological tower situated at Carrasco Airport in Montevideo (56°06′W, 34°42′S) through the National Climate Data Center database (Fig. 2a). Carrasco winds were measured at tower height of z = 10 m in an urban area located 5 km from the coast. Comparisons to QuikSCAT winds reveal a correlation between the datasets of R = 0.76, but a tendency of Carrasco winds to underestimate the strength of ocean winds. Based on these comparisons, Carrasco observed winds (U_{obs}) were adjusted for winds speed according to: $U_{adj} = 1.25U_{obs} + 0.5$. Wind stress was computed following the procedure outlined in Large and Pond (1981).

Hourly sea-level information for Punta Lobos (56°15.4′W, 34°54.2′S) was provided by the Uruguayan Navy in a total of 3 months of sea-level data for summer and 3 months for winter. Harmonic analysis was performed in order to separate the lower frequency fluctuations for interpretation (Pawlowicz *et al.,* 2002). Observed subtidal fluctuations were up to 2 orders of magnitude larger than tidal amplitudes and accounted for ~89% of sea-level variance in Uruguay coast, compared to ~11% from tides.

3. Results

a. Wind forcing and subtidal shelf circulation

i. Seasonal and synoptic wind fields. The wind variability in southeastern South America features a seasonal cycle that is strongly linked to the position and strength of the Atlantic subtropical high pressure system (Castro and Miranda, 1998). This cycle is well described by mean sea-level pressure and the surface winds derived from the NCEP Reanalysis data set (Kalnay *et al.,* 1996). In the austral winter (Jun, Jul, Aug) the South Atlantic high-pressure center has its maximum near 28S (Fig. 4a). Near the coast southwesterly winds of ~0.05 to 0.1 Nm^{-2} force the shelf from Mar del Plata, Argentina (40S) to Santa Marta in south Brazil (29S). Westerly winds become more dominant farther offshore. In the austral summer the atmospheric mean circulation changes as the South Atlantic high-pressure cell migrates southward (~32S). East-northeast winds become the prevailing winds along the southern Brazil, Uruguay and Argentina between 18S and 40S (Fig. 4b).

Despite the general pattern of these seasonal wind fields, the Southeastern South Atlantic experiences high temporal variability of winds due the passage of cyclones produced from baroclinic and lee topographic instability of the Westerlies (Gan and Rao, 1991). Synoptic atmospheric systems frequently disrupt the seasonal patterns described above. More specifically, during both of our surveys in the winter of 1999 and the summer of 2000 eastward propagating high-pressure systems past our study area. Wind fields derived from QuikSCAT revealed that strong (0.07 and 0.12 Nm^{-2}) northeasterly winds caused upwelling during the winter (Fig. 4c) and the summer (Fig. 4d) surveys.

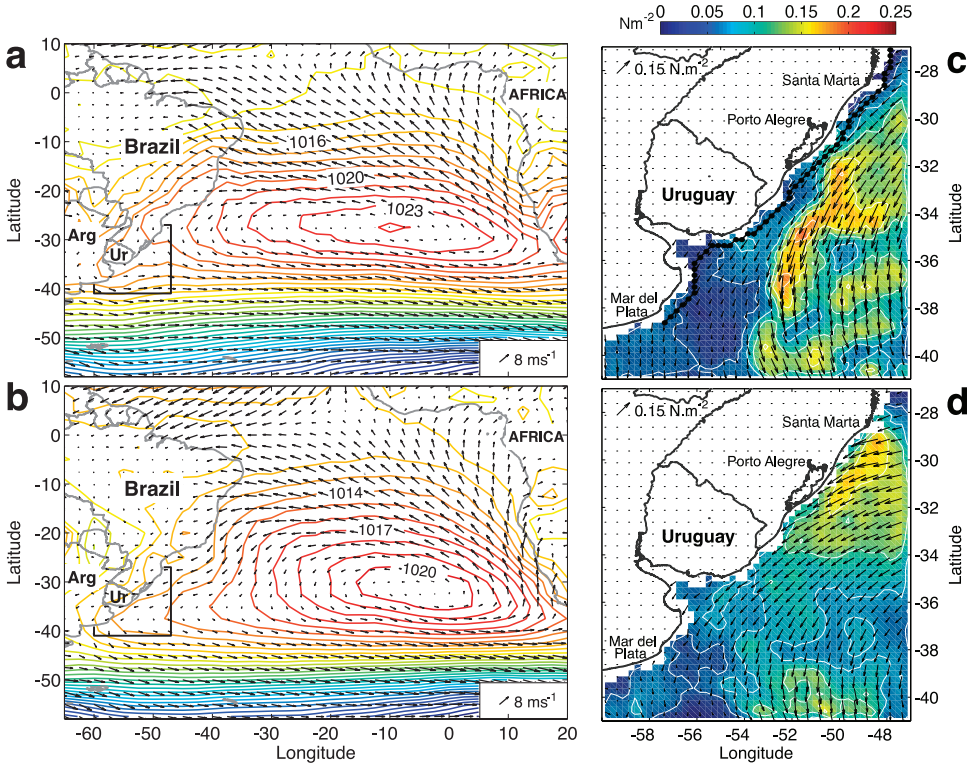

Figure 4. (a) Winter (Jun, Jul, Aug) and (b) summer (Dec, Jan, Feb) sea-level pressure (mb) and surface winds (ms^{-1}) derived from NCEP Reanalysis (Kalnay *et al.,* 1996) for the period of 1999 to 2007. The square in (a) and (b) indicates the region shown in (c) and (d). QuikSCAT mean wind stress (Nm^{-2}) fields for the winter event of August 18 to 20th, 1999 (panel c) and the summer event of January 29th to February 1st, 2000 (d). For clarity of exposition QuikSCAT vectors are plotted every two grid points (dx,dy ~ 50 km). Bullets connected by a continuous line in (c) are QuikSCAT points used in the graphs of Figure 5a (see text for details).

The evolution of these events throughout the study region are shown on Figure 5a, where we plot the along-shelf wind component (39° from true north) as a function of time and distance along the shelf. Winds generally blow in the same direction along the entire shelf from Mar del Plata, Argentina (MP) at ~38S to Santa Marta Cape, Brazil (SM) at 28S (Fig. 5a) and were upwelling favorable for the entire shelf during both periods of observation.

In Figure 5b we display wind vectors from Carrasco, Montevideo to illustrate the differences between these periods. Winter winds were more energetic and more variable than summer winds. More specifically, the upwelling-favorable wind event during the summer survey was longer, (8.4 days) and weaker ($\tau shelf \sim -0.1$ Nm^{-2}) as compared to the shorter (~4.2 days) and stronger winter event ($\tau shelf \sim -0.18$ Nm^{-2}). In the winter, a

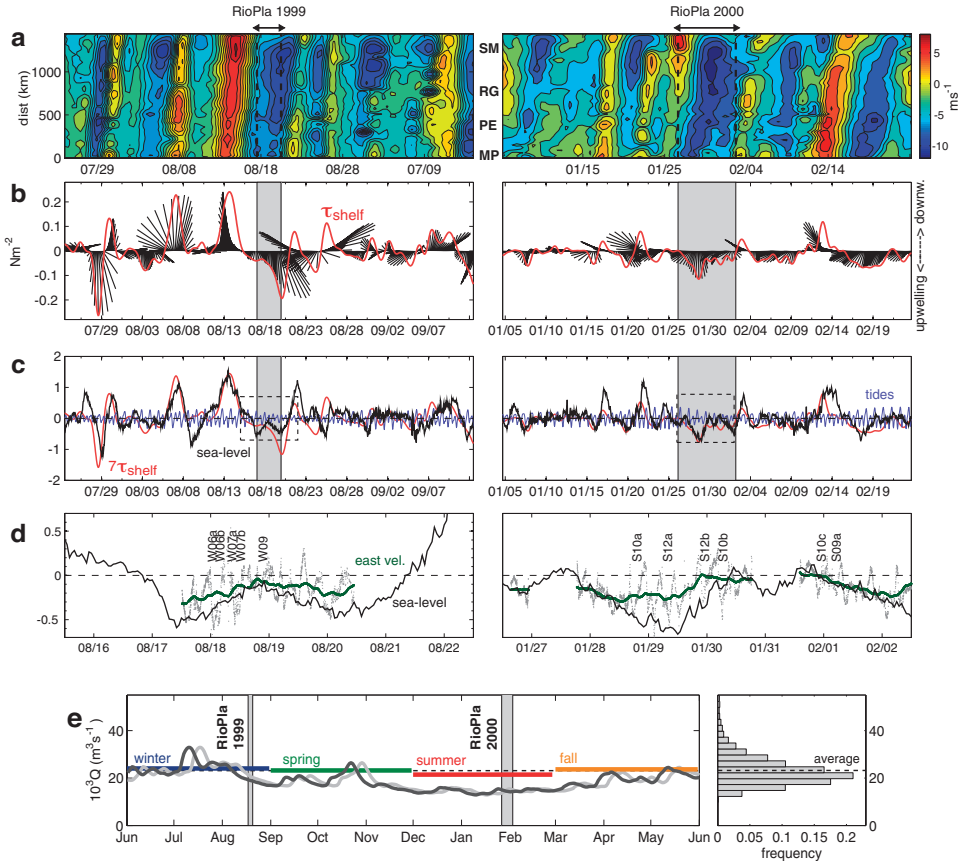

Figure 5. (a) Along-shelf winds as function of time and distance. Labels indicate geographical positions: Mar del Plata (MP), Punta del Este (PE), Rio Grande (RG) and Santa Marta (SM). QuikSCAT points used are shown on Figure 4c. Red colors indicate southwesterly winds and blue colors northeasterly winds. (b) Carrasco low pass filtered wind stress for winter (left) and summer (right panel). The red line is the along-shelf component (τ_{shelf}, 39° from true north). (c) Sea level from Montevideo and along-shelf winds (red line, $7 \times \tau_{shelf}$). The blue line depicts astronomical tides, while the subtidal sea-level component is in black. (d) Depth averaged ADCP detided zonal velocity (gray dots) and subtidal sea level (black). Negative values indicate westward flow. The green line is a 7-hour moving average applied to the zonal ADCP velocity data. (e) Plata river outflow from June 1999 to June 2000 and discharge histogram derived from the historical dataset (1975–2005). Colored horizontal bars indicate the seasonal discharges, whereas the black dashed line shows the historical mean. River flow is computed as the sum of Chapetón and Paso de los Libres stations shown as a dark gray line. The light gray line corresponds to the same series lagged in one week.

strong downwelling wind event ($\tau shelf > 0.2\ \mathrm{Nm}^{-2}$) preceded our experiment, while for the summer the preceding downwelling event had more modest wind speeds over a smaller shelf area (Fig. 5a).

ii. Sea level and currents time variability. Sea-level variations along the coast of Uruguay are dominated by subtidal oscillations whose amplitudes are 2–3 orders of magnitude larger than tidal sea-level oscillations (Fig. 5c). Furthermore, subtidal sea-level oscillations correlate well with along-shelf winds as expected by a coastal Ekman flux divergence, e.g., downwelling-favorable (southwesterly) winds raise sea level while upwelling-favorable (northeasterly) winds depress it. Maximum correlation of $R = 0.74$ between winds and subtidal sea level occur when the along-shelf winds (projected to an axis at 39° from North) are lagged by 7 hours relative to sea level.

We observed a similar response of shelf currents to wind forcing. Assuming that the detided, depth-averaged zonal ADCP velocity component represents along-shelf currents over the entire stretch of coast, we compare ADCP velocities with subtidal sea-level observations in Figure 5d. The short peaked velocity fluctuations shown represent across-shelf variability of alongshore detided currents. A moving average (7 hours) of the ADCP data removes these fluctuations and highlights the close agreement of low-passed ADCP currents to the sea level variability (Fig. 5d). The lowest coastal sea level was associated with the strongest poleward currents, consistent with a barotropic shelf response to wind forcing for which across-shelf pressure gradients are balanced by along-shelf currents, i.e., a geostrophic balance. These shelf currents were dominantly poleward during the ADCP observation periods, near 3.5 days for winter and ~4.5 days for the summer cruise.

iii. Subtidal velocity fields. The effect of these upwelling events upon the subtidal shelf circulation is further complemented by Figure 6 where we plot the detided, depth-averaged current observations correspondent to the winter (panel a) and summer (panel b) surveys. In both seasons we found southward currents, which generally follows the isobaths. The flow intensity was large over the inner shelf, ~ 0.35 m s^{-1}, reducing to 0.1 m s^{-1} offshore. The canyon did not alter the depth-averaged circulation substantially, although some of the higher velocities were found along its axis.

Vertical sections show this intensification near the canyon slope for both winter (Fig. 7) and summer (Fig. 8). Higher velocities (>0.4 m s^{-1}) along the canyon axis occurred in the northern transects (e.g. W13, S12) weakening along its southward path toward the estuary. During the winter, the core of this current was nearly 15-km wide, while for summer the current structure was much wider and less sheared.

The most significant horizontal shear of along-shelf currents was observed for the winter sections between Punta del Este and Cape Santa Maria. In these transects the currents reversed their direction offshore, with northward velocities on the order of 0.2 m s^{-1} near the surface (Fig. 7, sections W07b to W10).

A good visualization of the subtidal, depth-averaged velocity fields was obtained when we applied a multivariate optimum interpolation of the horizontal flow field (Bretherton *et al.,* 1976). Here we computed the summer/winter streamfunction maps from the entire ADCP surveys, so the data coverage is better than shown on Figure 6a,b. Both maps cover

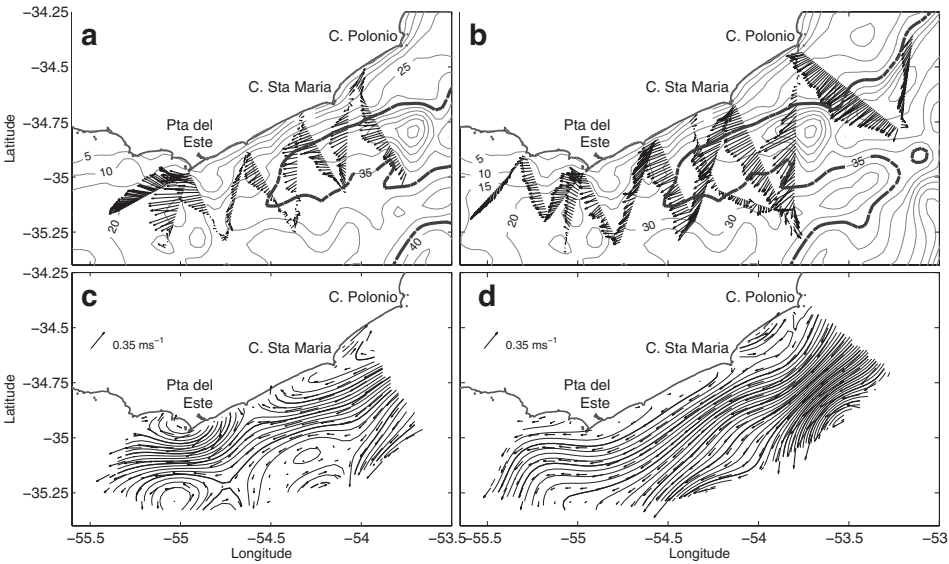

Figure 6. Detided ADCP depth averaged currents (arrows) for (a) winter 1999 and (b) summer 2000 cruises. Contour lines indicate depths in meters. The canyon rim (35-m isobath) is displayed as a thick line. Residual stream function and interpolated vector fields are shown in (c) for winter and (d) for summer.

periods under upwelling favorable winds and dominantly poleward flow, i.e. no reversal was observed in the along-shelf circulation. Figures 6c and 6d show residual stream function maps and their interpolated vectors fields; $u = -\partial\psi/\partial y$, $v = \partial\psi/\partial x$, which emphasize different aspects of the Uruguay upwelling circulation. Both streamfunction maps mark the presence of a poleward jet crossing the Uruguay inner-shelf during the surveys. The current starts at Cape Polonio in the northern side, flowing poleward all the way to Punta del Este in the southern domain. Past Punta del Este, the current is deflected by the local estuarine bathymetry, apparently flowing southward across the mouth of the Plata estuary. Nearshore cyclonic cells are observed downstream of Cape Polonio, Cape Santa Maria and Punta del Este. Their positions in relation to these coastal capes suggest the occurrence of recirculation eddies induced by the coastal headlands. Away from the shoreline, the presence of Plata bank suggests a partial deflection of the mid-shelf flow southwards, along the bank offshore slope (Fig. 6d).

b. Temperature and salinity fields

Although the alongshore circulation patterns were relatively similar in summer and winter, the corresponding temperature and salinity fields were distinctly different. We here describe the response of the Rio de la Plata river plume to the strong winter and to the more moderate summer upwelling winds.

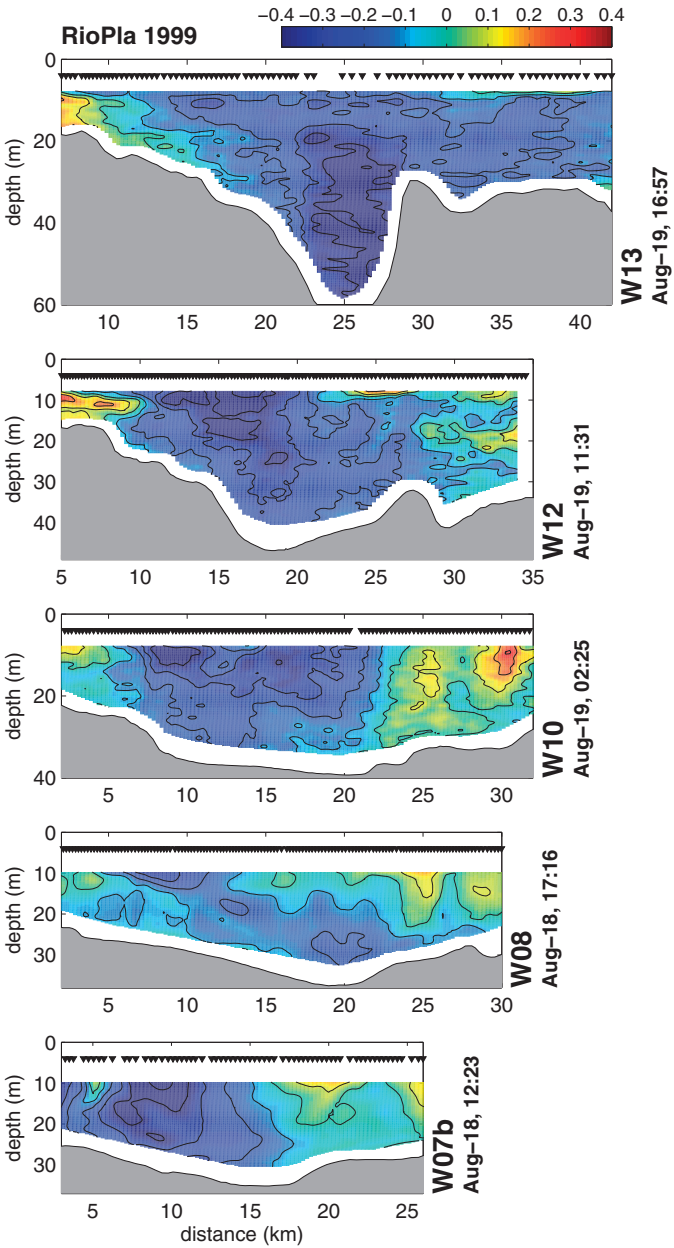

Figure 7. Winter 1999 detided along-shelf velocity transects. Blue (red) colors indicate upshelf (downshelf) flow in reference to the coast orientation of Punta del Este (W07b) to Cape Santa Maria (W13) (~69° from true north). Contour velocity increment is $\delta V = 0.1$ m s^{-1}.

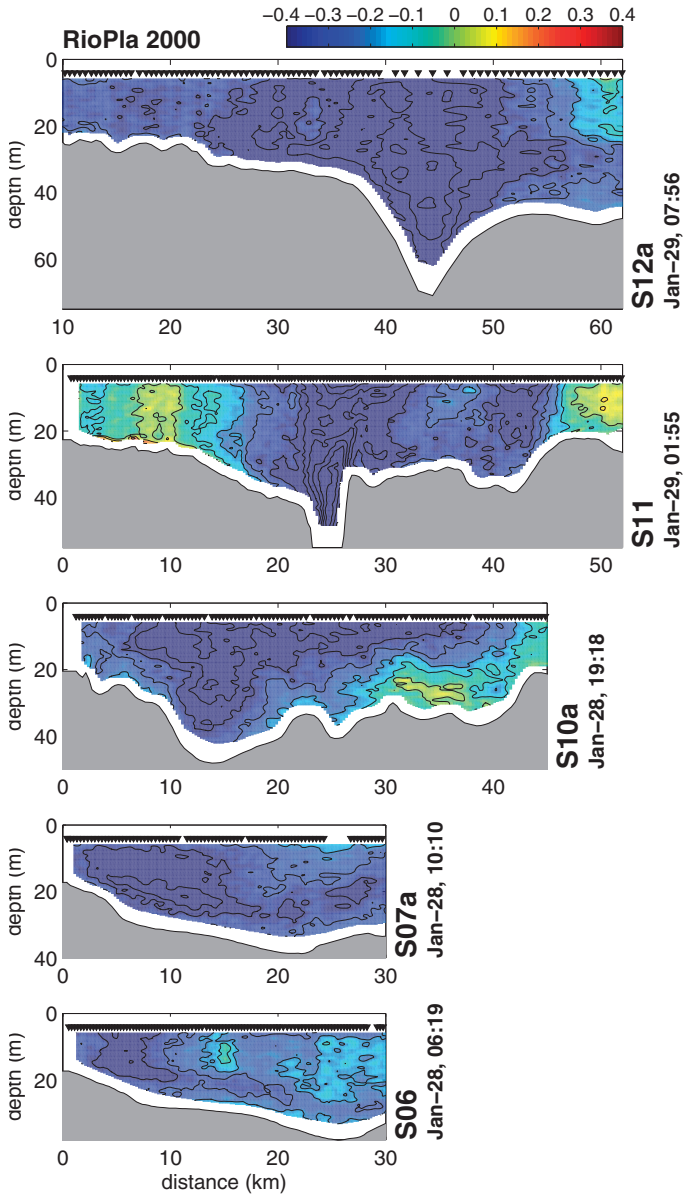

Figure 8. Summer 2000 detided along-shelf velocity transects. Blue (red) colors indicate upshelf (downshelf) flow, referent to the shelf orientation between Punta del Este (S06) to Cape Polonio (S12a) (∼69° from true north). Contour velocity increment is $\delta V = 0.1$ m s^{-1}.

i. Plata plume winter response to upwelling winds. The winter period was characterized by relatively strong discharges and winds. Plata outflow averaged Q ≈ 18910 m^3 s^{-1} during

the 1999 survey, or near Q ≈ 20600 m^3 s^{-1} if one considers a week-long delay between upstream river gauge measurements and the actual freshwater delivery to the estuary (Fig. 5e). This discharge magnitude was lower than mean winter discharge of 24,046 m^3 s^{-1}, as shown in Figure 5e, but still higher than the observed spring and summer outflows.

This buoyancy flux would imply strong equatorward buoyancy-driven coastal current along the Uruguayan and Brazilian shelves in the absence of winds. However, our observed ADCP velocity fields indicated that the plume was being advected poleward by shelf currents. The hydrographic observations revealed a slow cross-shelf response of the coastal plume.

Prior to our winter surveys strong downwelling winds ($\tau shelf \approx 0.2$ Nm^{-2}) blew from south-southeast for nearly 3.5 days. In fact, the horizontal surface salinity fields earlier sampled in August 14th 1999 (before the start of ADCP operations), demonstrate the Rio de la Plata river plume to be well defined and constrained by the downwelling winds (shown as stick plots) near Punta del Este (Fig. 9). As the surveys progressed from south-west to north-east, these winds relaxed and changed to upwelling-favorable. Figure 9a shows the changes of the Carrasco winds and the resultant spatial distribution of the surface buoyant plume.

More specifically, Plata waters gradually detached from the coast and became modified due to the dominant poleward wind induced currents. Surface salinities varied from less than S ~ 4 off Montevideo to about S ~ 20 over the shelf, while off Cape Santa Maria we find relatively saltier plume waters with S > 26 nearshore while near Punta del Este an intrusion of saltier shelf waters is suggested by the velocity fields (Fig. 6c). This could have been promoted by an anticyclonic eddy located offshore of this cape.

As expected for strongly stratified plumes, bottom salinities bore little resemblance with surface salinities. Fresh bottom waters were constrained to the estuary, while relatively homogeneous saltier waters (S > 32) occupied the bottom in the inner-shelf area between Punta del Este and Cape Santa Maria (Fig. 9b). The bottom intrusion of ambient shelf waters toward the estuary was limited to the ~20-m isobath, as pointed out previously by Guerrero *et al.* (1997). These bottom shelf waters, as shown by the temperature-salinity correlations of Figure 2b, are diluted Subantarctic waters (Subantarctic Shelf Waters, SASW) with salinities around S ~ 33.8 and temperatures of about T ~ 10.3°C. At the surface this is nearly indistinguishable from estuarine water temperatures, hence AVHRR SST observations may miss the signals associated with winter upwelling.

Vertical plane views are shown for a 300-km long along-shelf salinity transect in Figure 9c, and for five cross-shelf salinity (and temperature) sections in Figure 10. These sections reveal that as the buoyant plume detaches from the coast, it also becomes progressively thinner forming a cap of fresher waters (S < 18) that nearly isolate the bottom from the action of winds.

Figure 10 also shows how the circulation varies from downwelling to upwelling. During downwelling-favorable winds on August 15th isohalines slope upward toward offshore for section W04 (Fig. 10). As the winds changed to upwelling-favorable, the plume evolved in

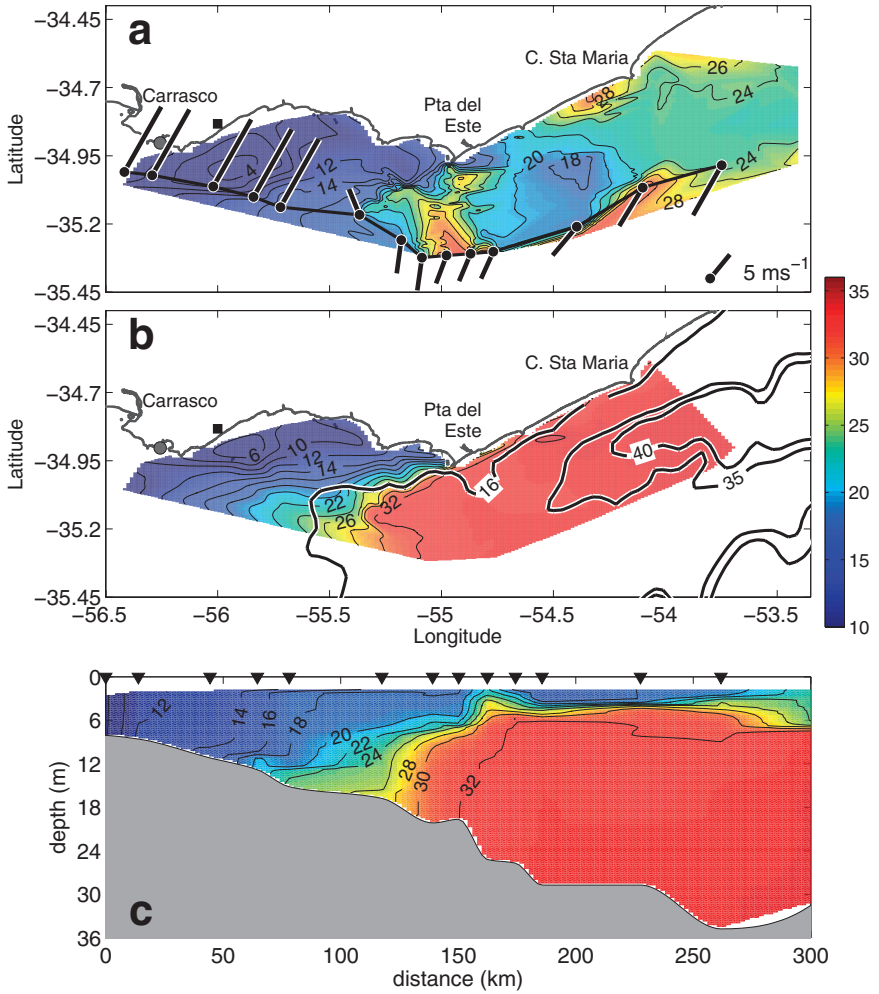

Figure 9. Winter salinity fields for (a) surface, (b) bottom, and (c) as a section along the coast. Salinity is depicted by the color scale and thin contour lines (increment is $\delta S = 2$). Upper panel bullets indicate selected CTD stations used for vertical panel and the sticks indicate winds observed during the survey. Wind observations shown are derived from Carrasco. Distance on (c) is oriented from the estuary (0 km) to the shelf (300 km).

response to the offshore transport of surface waters and the saltier, deeper onshore return flow. This process separated the Rio de la Plata plume from the bottom and promoted the intrusion of relatively colder waters, which, however, did not outcrop to the surface. In a final stage, the plume became a freshwater lens partially detached from the coast (Fig. 10, W13).

Following Brainerd and Gregg (1995), we further estimated the mixed layer thickness from the winter density fields. The surface mixed layer (sml) was determined by finding the

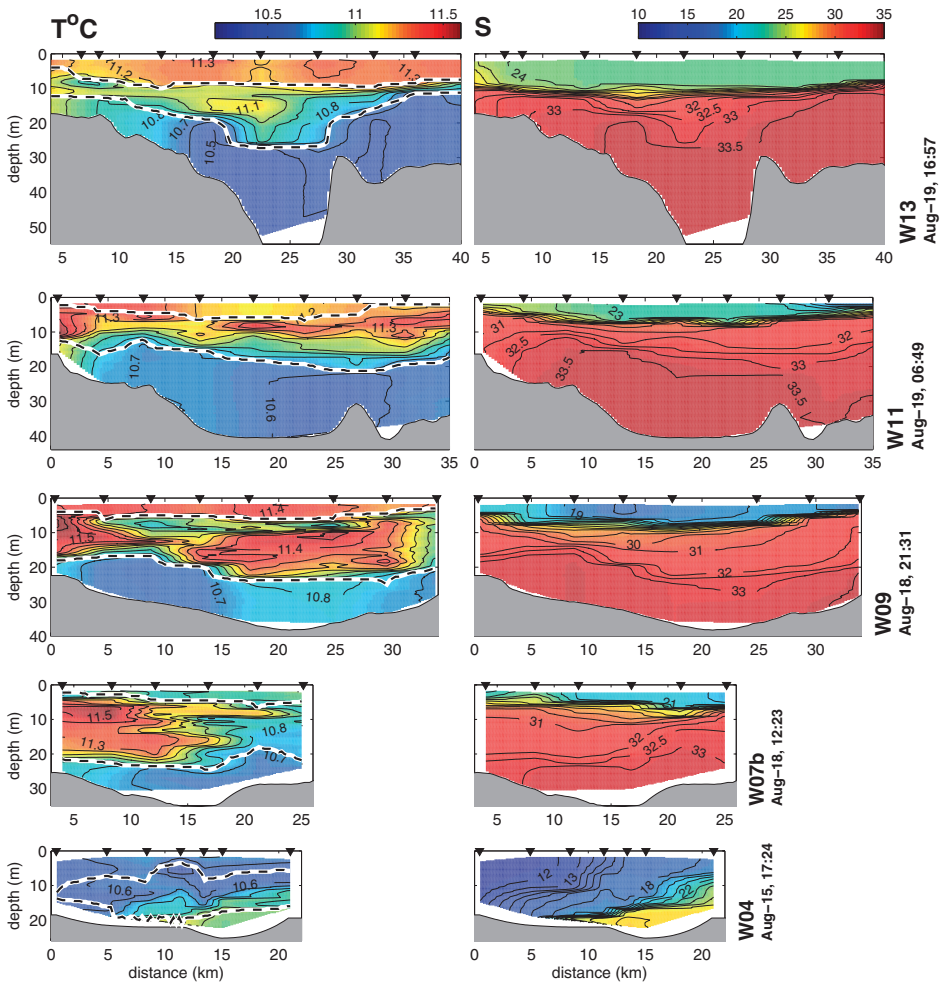

Figure 10. Winter cross-shelf transects of temperature (left panels) and salinity (right panels). Each row shows a different transect from north (top) to south (bottom). The transects names and sampling date are shown on the right panels and the transect positions are indicated on Figure 3a. Distance offshore is in kilometers and depth is in meters. Color scales are shown on the top of columns. Contour intervals are $\delta T = 0.2°C$ for temperature and $\delta S = 1$ for salinity. Surface and bottom mixed layer depths are indicated by dashed lines.

depth where the difference to the surface density (ρ_{surf}), computed as $\Delta\rho = \rho(z) - \rho_{surf}$, achieved a threshold of $\Delta\rho$. A set of tests was performed to evaluate the sensibility of the choice of $\Delta\rho$. We found that changing this threshold in the interval of $0.05 \leq \Delta\rho \leq 0.5$ did not change dramatically the results. We choose the value of $\Delta\rho = 0.3$ kg m^{-3} however, because it best represented the mixed layer from the joint analysis of density and cross-shelf velocity sections. The bottom mixed layer (bml) was estimated in a similar way

with $\Delta\rho = \rho_{bott} - \rho(z)$ and ρ_{bott} representing the bottom density. Here we display these mixed layer depths as dashed lines in Figure 10. They reveal the shallowness ($5 < \delta_{sml} < 10$ m) of the winter sml due to the high stratification imposed by the freshwaters from the Rio de la Plata. On the other hand, the bottom mixed layer was thicker ($10 < \delta_{bml} < 20$ m) and characterized by relatively colder waters.

Between the fresh upper and cold bottom mixed layers, we found a thick and well-stratified interior. This layer was characterized both by warmer waters and occasional temperature inversions due to relatively cooler waters near the foot of the sml. This interior layer became thinner from near $\delta_{int} \sim 20$ m at W07b to $\delta_{int} \sim 10$ m at W13. Although our observations do not cover regions shallower than 15-m depth, we find that the horizontal buoyancy sustained a well-stratified inner shelf interior, even with large frictional effects. This situation is similar to that reported by Garvine (2004) for the inner shelf off New Jersey where the Hudson Coastal Current provides buoyancy.

ii. Summer upwelling and the coastal subtropical intrusion. The summer cruise was characterized by weak discharges, on the order of $Q = 14500$ m^3 s^{-1}. This magnitude contrasts with the winter cruise, and specially with the expected seasonal average. As show in Figure 5e, river outflow was nearly 40% lower than the climatological summer mean. Furthermore, not much buoyancy signal was being delivered downshelf. The analysis of the entire summer CTD data revealed that most of the fresher waters ($S < 20$) were being driven upshelf, along the Argentinean side of the estuary. Figure 2b illustrates this with gray crosses which denote temperature salinity correlations of RioPla upshelf stations along the Argentinean side of the estuary, while black circles indicate the RioPla downshelf stations explored here; along the coast of Uruguay. Figure 2b shows that diluted subtropical waters ($S > 30$) were prevalent along the Uruguayan coast, while most of the Plata fresher waters ($S < 30$) were present upshelf. The occurrence of upshelf delivery is also supported by the SST image of Figure 1.

Nevertheless, we find traces of the Rio de la Plata plume waters ($S < 33.5$) off Uruguay near Punta del Este area and offshore of Cape Santa Maria (Fig. 11a). Most surprisingly, along most of the coastline we find a well-defined intrusion of salty and warm subtropical waters ($S \sim 34.2$; $T \sim 24.6$°C) (Fig. 11a,b). The intrusion, induced by poleward currents, extended ~40 km across and ~150 km along-shelf. The origin of these waters is likely southern Brazil as we find the warmest and saltiest waters near the bottom off Cape Polonio, as shown by the along-shelf transect of Figure 11c and also by the bottom temperature distribution of Figure 11d. South of Cape Santa Maria, the subtropical intrusion separates from the bottom, occupying the upper 20 m of water column (Fig. 11c) only. The structure of this warm and salty intrusion narrows and gradually veers offshore as it approaches Punta del Este (Fig. 11a).

On the shore side of the subtropical intrusion the sea surface temperature reveal the outcrop of colder waters ($T \sim 19$°C) in the coastal area adjacent to Cape Santa Maria and Punta del Este (Fig. 11b). This surface expression of local upwelling extended nearly

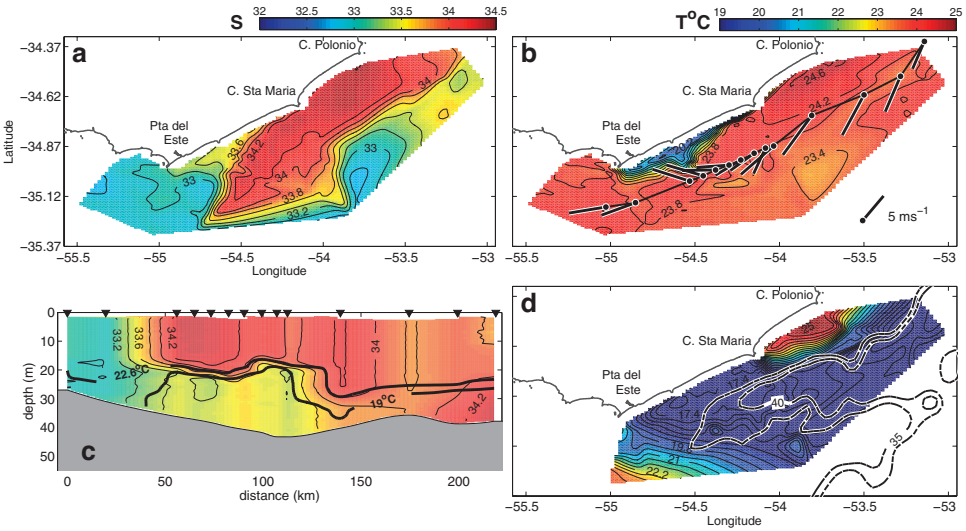

Figure 11. Summer thermohaline fields. Surface (a) and along-shelf (c) salinity distributions are depicted with $\delta S = 0.2$ contour increments. Surface (b) and bottom (d) temperature fields have a contour interval of $\delta T = 0.4°C$. The bullets at panel b indicate the CTD casts used for panel c, with winds measured from Carrasco indicated by sticks.

20 km offshore and 80 km alongshore. In contrast, the spatial extent of cold bottom waters ($T \sim 17.5°C$) was larger and occupied most of the mid-shelf areas; in particular the region of the canyon bathymetry and the nearshore region south of Cape Santa Maria (Fig. 11d). The thickness of the subsurface cold intrusion varied from 10 to 20 m, as shown in Figure 11c by the $T = 19°C$ and $T = 26°C$ isotherms. These are Subantartic Shelf Waters (SASW) (Fig. 2b).

Figure 12 offers a complementary view of the summer thermohaline structure as the vertical temperature and salinity cross-shelf sections reveal how the 15 to 20-m thick warm upper layer ($T > 23°C$) nearly caps the entire study region. In the northern transect (S12b) this layer reaches the bottom in the nearshore area off Cape Polonio. The lower layer is characterized by cold waters ($T < 18°C$), which occupies the deepest parts of Plata canyon. In the middle sections we observe how these cold bottom waters reach toward the shore outcropping to the surface (see Fig. 12, S07b to S10c). Offshore of this front the salinity sections reveal not only a defined core of the subtropical intrusion, but also well mixed Plata waters, sitting on the top of La Plata bank (Fig. 12, S09 and S10c).

Unlike the winter density field that was largely controlled by salinity, the summer density field was largely controlled by temperature. Hence the limit of the sml coincides with the location of the thermocline (dashed lines in Fig. 12). These upper and lower mixed layers leave very little room for the development of a stratified interior, again in contrast to the winter situation. The interior layer for summer was often less than $\delta_{int} \sim$ 3-m thick and surface and bottom layers were frequently in close contact; in the northern domain the

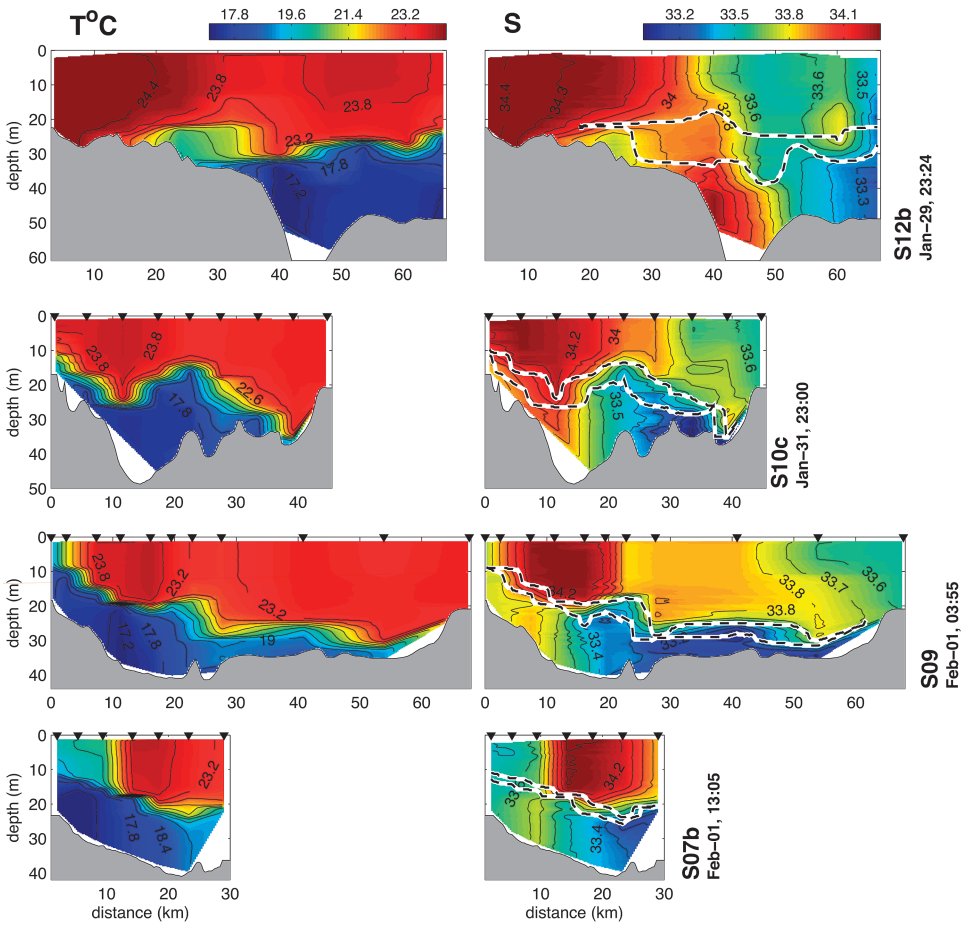

Figure 12. Summer transects of temperature (left panels) and salinity (right panels). Each row shows a different transect from north (top) to south (bottom). Transects names and dates are indicated on right and their positions are in Figure 3b. Distance offshore is in kilometers and depth in meters. Color scales are shown on the top of columns and contour intervals are $\delta T = 0.4°C$ for temperature and $\delta S = 0.2$ for salinity. Surface and bottom mixed layer depths are indicated by dashed lines.

mixed layers merged nearshore (transect S12b) and in the intermediate region (S09 and S10) the surface and bottom mixed layers merged into one mixed layer offshore, above La Plata bank (depths $\sim$ 20 m).

In summary, during the summer we find two distinct frontal structures off Uruguay. The first was the nearshore temperature front between Punta del Este and Cape Santa Maria, which separated cold upwelled waters from warm surface waters intruding from southern Brazil. The second was a salinity front positioned offshore and formed by fresher waters containing Rio de la Plata plume waters ($S < 33.6$).

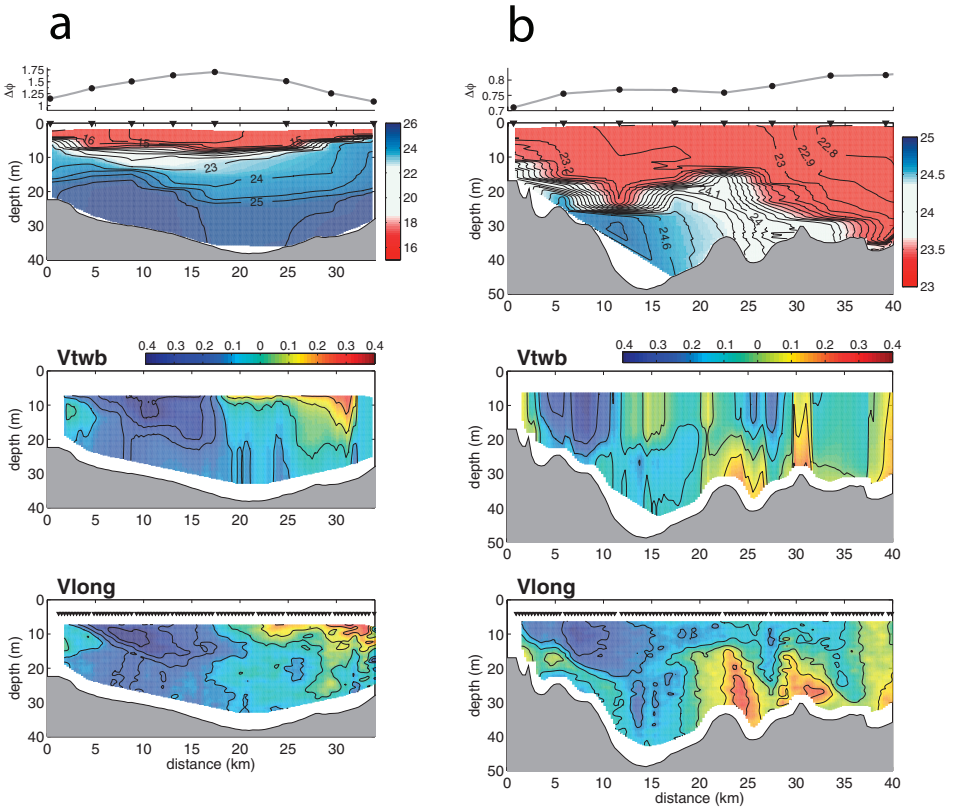

Figure 13. Transects of density (upper panel), thermal wind velocity, V_{twb} (middle) and ADCP along-shelf velocity (lower panels) for (a) winter transect W09 (Aug-18, 21:31) and (b) summer transect S10c (Jan-31, 23:00). The upper graphs above the density panels are the geopotential anomalies derived from CTD casts (bullets) and interpolated field (gray line). Density contour increments are $\delta\sigma = 1$ kg m^{-3} for winter and $\delta\sigma = 0.2$ kg m^{-3} for summer. Velocity increments are $\delta V = 0.1$ m s^{-1} in all sections. Large triangles mark CTD casts positions and small triangles the ADCP observations. Velocity components are perpendicular to each transect orientation, with blue colors indicating poleward currents. Note that different color scales are applied for the winter and summer density fields.

c. Analysis of velocity fields

i. Geostrophy of baroclinic flow. Here we examine the baroclinic flow component of Uruguay along-shelf currents, as in both seasons we found characteristics that were consistent with the observed density field. During the winter, density fields were characterized by strong vertical and horizontal gradients setup by the buoyant lens of freshwater ($\sigma < 24$ kgm^{-3}). Because of its low density and configuration, the sea surface adjusts to a dome-like configuration sitting higher in the center region of the plume, as shown in terms of the surface geopotential anomaly ($\Delta\phi$, m^2 s^{-2}) in Figure 13a, which was computed in

reference to the 20 dbar isobar. Surface geostrophic currents are proportional to the slope the surface geopotential anomaly, $v \sim f^{-1}\delta\Delta\phi/\delta x$. In agreement, we find poleward and equatorward near-surface currents respectively on the nearshore and offshore sides of the plume, as shown by the ADCP transect on Figure 13a (lower panel).

These surface currents slow down with depth due to the increasing and opposing baroclinic pressure field. In order to inspect the consistency of the observed vertical shear to that described by a thermal wind balance (TWB), we further integrated the density field to obtain a velocity profile (V_{twb}):

$$V_{twb}(x, z) = V_{ref}(x, z_{ref}) + \int_{zref}^{z} (-g/\rho_o f)\frac{\partial \rho}{\partial x}\, dz'.$$

Here V_{ref}, is the reference velocity at depth z_{ref}, which we take as the lower ADCP measurement. The resultant synthetic field compares well to the observed currents, as shown by the middle and lower panels of Figure 13a. Horizontal density gradients generate negative and positive velocity shear respectively on the nearshore and offshore sides of the plume. This is consistent to the surface poleward jet we observe near 5 to 15 km from coast and to a northward flowing current found farther offshore (25–35 km). A few winter sections (not shown) also reveal a weak equatorward subsurface flow nearshore where the isopycnals slope downward to the coast.

For the summer situation, the along-shelf flow was initially dominantly barotropic. As seen by Figure 5d, peak flows occurred January 29th, 2000 in the nearshore region off Uruguay. During this period, the baroclinic effect of the density field upon currents was less evident from observations. As the upwelling-favorable winds diminished, however, the barotropic currents weakened and the dynamic effect of the density field became more evident in the ADCP transects (Fig. 13b). Specifically, the ADCP shows a poleward jet nearshore associated with the upwelling thermal front and another weaker jet associated with Plata reminiscent fresher waters. These surface geostrophic currents were consistent to the slopes of the surface geopotential anomaly, which was computed in reference to the 16 dbar isobar (Fig. 13b, top graph). The poleward jets are positioned along the slopes of the surface geopotential. The thermal wind fields, shown on the lower panels of Figure 13b also matched well with velocity observations, displaying similar vertical shear and structure in comparison to the ADCP currents.

These winter and summer situations agree with earlier observational studies, that likewise, found that TWB explain the coastal currents shear well in regions as shallow as 15-m depth (Garvine, 2004; Yankovsky *et al.,* 2000).

ii. Cross-shelf velocity fields. In order to explain the phenomena that established the observed density fronts, we investigated the structure of the across-shelf circulation from the towed ADCP observations. Since summer velocity measurements were better suited for

this analysis, we used this record to map the circulation near the upwelling center off Uruguay.

We focused our analyses on the area between Punta del Este and Cape Santa Maria (see Fig. 3b for location) and we describe the general circulation in terms of surface and bottom maps by vertically averaging the upper and lower 10 m of water column of the summer ADCP surveys (Fig. 14 a,b). The lower layer is characterized by generally southward currents with enhanced cross isobath flow (Fig. 14a). The stream function indicates that a substantial portion of the canyon flow steers toward the coast, converging between Punta del Este (PDE) and Cape Santa Maria (CSM). The across-shelf change in depth from the canyon talweg ($\sim$75 m) to the inner shelf ($<$20 m) occurs within $\sim$15 km. In contrast, currents at the surface diverge from the area between these capes, thus facilitating the poleward drift of warm subtropical waters advected from the southern Brazil (Fig. 14b).

Two ADCP transects crossing the canyon axis reveal the vertical structure of the cross-shelf circulation (Fig. 14 c,d). The sections evidence the bidirectional nature of the summer cross-shelf circulation, with an strong upper layer flow of $\sim$0.2 m s^{-1} offshore, and a bottom return flow of 0.10 to 0.25 m s^{-1}. The bottom circulation is consistent with the dynamics of a bottom Ekman layer forced by a geostrophic flow, i.e. a southward along-shelf current driving cross-isobath transport. Note that the presence of intensified bottom flow also coincides with the location of the steepest bottom slope and thinnest bottom mixed layer (Fig. 14c).

The winter circulation was in few aspects similar to the scheme demonstrated for summer (Fig. 15). We did not obtain a clear picture of the sml circulation, because (a) the winter sml was thinner and (b) the ADCP tow was located deeper and thus missed most of the upper layer circulation. The salinity distribution, however, was consistent with an offshore transport in the fresh surface mixed layer. A thin surface Ekman layer would give initially large velocities from the Ekman scaling, $u \approx \tau/\rho hf \sim 0.3$ m s^{-1}, for an upper layer of h $\approx$ 8 m and winds of $\tau \sim 0.2$ Nm^2. Fortunately, the deeper circulation was better resolved. As during summer upwelling, bottom mixed layer contains the onshore flow during the winter (Fig. 15, W12).

Surprisingly, the interior stratified region accommodated a substantial part of the circulation. Velocity sections along with the CTD temperature profiles demonstrate the subduction of relatively warm (11.5°C) coastal waters within the near-shore plume front (Fig. 15, left panels). The vertical structure also indicates a measurable onshore flow of cold waters near the foot of the surface mixed layer. This situation was particularly clear on the section W09, as illustrated by the colder temperatures and onshore velocity near 10 meters depth (Fig. 15).

4. Discussion: The role of winds on shelf circulation

a. Along-shelf circulation

Our observations indicate that local winds were capable in the winter of 1999 and summer of 2000 to overcome the northward density driven currents established by the

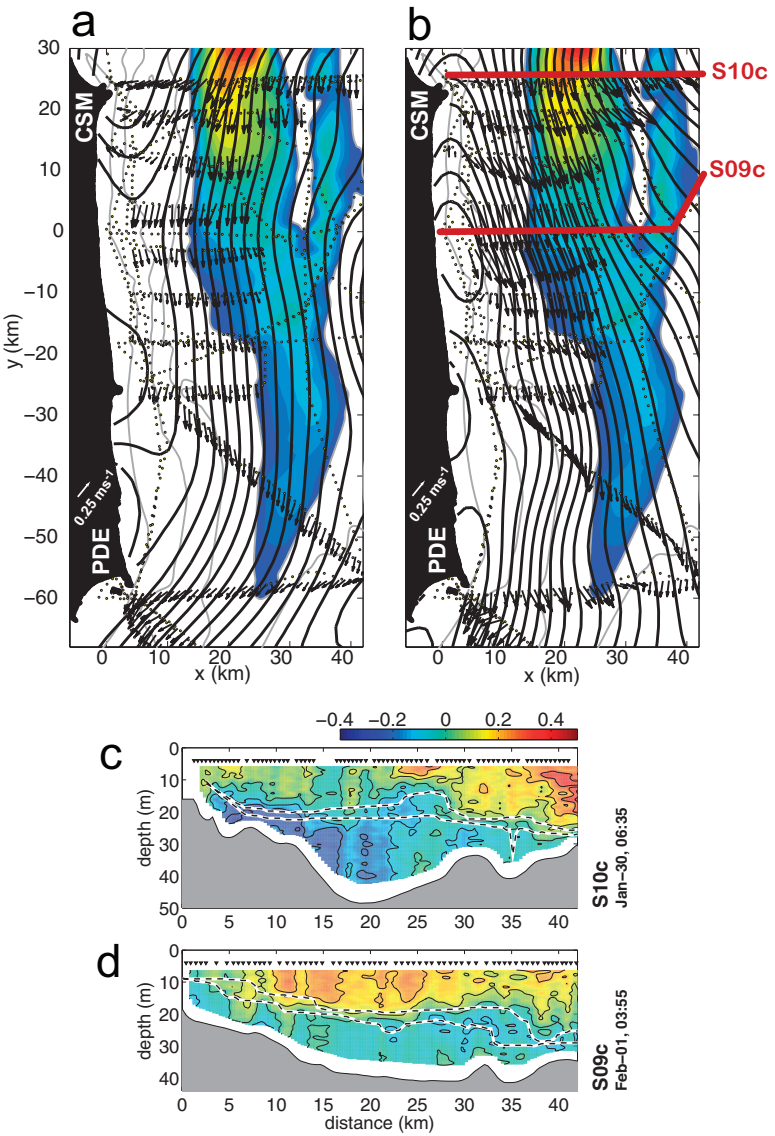

Figure 14. Summer 2000 stream function maps for (a) bottom and (b) surface along with ADCP observations (black vectors). The shelf topography is depicted by gray isobaths with 5-m increments. The color shade highlight Plata canyon, with blue colors indicating its canyon rim (35 m) and red colors its deeper regions (~60 m). Small dots indicate all velocity measurements used for interpolation. Transects of cross-shelf velocity for sections S10c and S09c are shown in (c) and (d) respectively, where offshore (onshore) velocities are indicated by red (blue) colors. Sections positions are indicated in (b). Map labels represent Punta del Este (PDE) and Cape Santa Maria (CSM). Maps (a) and (b) as shown were rotated in 69° from true north to facilitate exposition, so x-axis approximately grows southward and y-axis eastward.

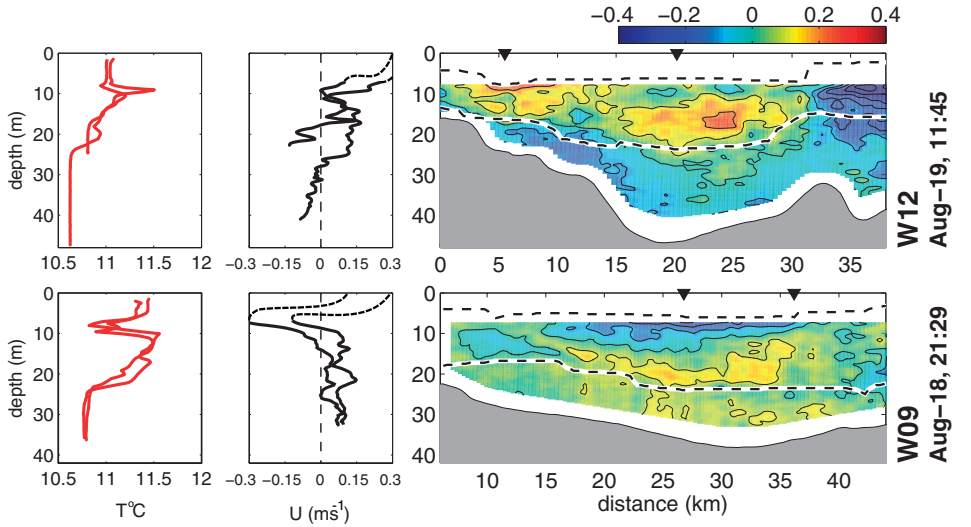

Figure 15. Winter 1999 across-shelf velocity transects (right panels) with temperature (left panels) and across-shelf velocity (middle panels) profiles. Velocity increment is $\delta V = 0.1$ m s^{-1}. Large triangles indicate profiles positions. Dash lines on velocity sections represent the surface and bottom mixed layer depths derived from the density fields. The dashed line drawn on the velocity profiles refers to a suggestion of the upper layer circulation lost by the ADCP measurements.

freshwater discharge from the Rio de la Plata. In the winter, despite the presence of the plume, the wind-induced currents carried previously discharged fresher waters southward along the Uruguayan coast. How frequent are such winds that overcome the buoyancy forcing of the Rio de la Plata plume? In order to answer this question we examine a yearlong history of a wind strength index (Whitney and Garvine, 2005) to discuss the along-shelf circulation. This index determines whether the along-shelf flow is in a wind-driven or a buoyancy-driven state. The ratio employed, $W_s = u_{wind}/u_{dis}$, is based on theoretical arguments that compare the magnitude of a frictionally adjusted wind-driven current, i.e., $u_{wind} = \sqrt{(\rho_{air}/\rho)(C_{10}/C_{Da})}\ U$ to a buoyancy-driven flow, i.e., $u_{dis} = (2g'_r Qf)^{1/4}/K$, where the parameters are the density of air $\rho_{air} = 1.2 \times 10^{-3}$ kg m^{-3}, the density of water, $\rho = 1025$ kg m^{-3}, the surface drag coefficient $C_{10} = 1.2 \times 10^{-3}$ and the bottom drag coefficient $C_{Da} = 2 \times 10^{-3}$. For the wind speed, U (m s^{-1}), we use low-pass filtered winds from Carrasco. The buoyancy velocity relates to the river discharge, Q and the plume Kelvin number, $K = L/R_{di}$, where R_{di} is the internal Rossby radius of deformation, $R_{di} = \sqrt{g'h}/f$ and L is the plume across-shelf length. The river reduced gravity is $g'_r = g\Delta\rho_r/\rho_a \approx 0.24$ ms^{-2} with $\Delta\rho_r = \rho_r - \rho_a$, where ρ_r is the density of river water and ρ_a is the density of ambient shelf waters. Analysis from previously published observations of Rio de la Plata plume suggest a Kelvin number within $K = 8$ and $K = 11$, as indicated from different hydrographic transects (Soares and Möller, 2001;

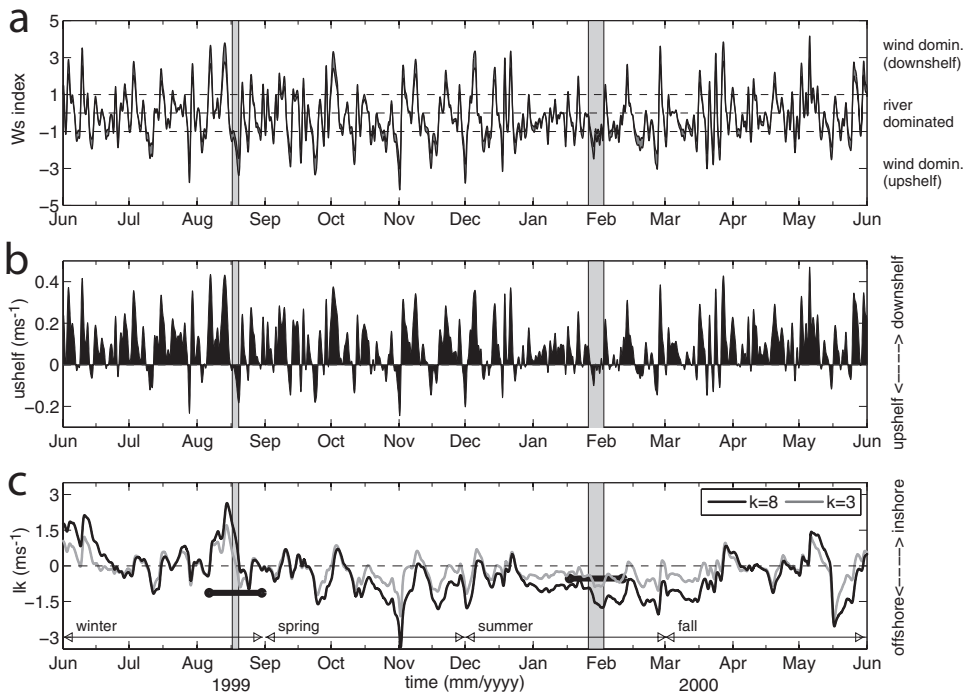

Figure 16. Time series of wind strength index, W_s (a) and along-shelf flow, u_{shelf} (b) from June 1999 to June 2000. Parameters were computed based on theoretical arguments developed in Whitney and Garvine (2005). W_s and u_{shelf} calculations use the wind component along 39N. (c) Wind impulse integral, Ik, calculated from a wind stress component that is parallel to the upwelling center, located between Punta del Este and Cape Santa Maria (~60° from N). This last was computed based on exponential decay factors of three (gray) and eight days (black). The thick black horizontal bars indicate typical summer and winter stratification thresholds for the outcrop of bottom waters to the surface as predicted by a simplified upwelling model (Csanady, 1977).

Möller *et al.,* 2008; Piola *et al.,* 2008). The computation of this nondimensional number is described in the Appendix.

Figure 16a shows one year of the wind strength index computed from a time series of winds, $U(t)$ and river discharge, $Q(t)$. Here we plot W_s as a filled curve, representing the upper and lower bounds of our estimate (i.e. $K = 8$ and $K = 11$). We also indicate by dashed lines when the plume is dominantly buoyancy-driven ($|W_s| < 1$) and when it is dominantly wind driven ($|W_s| > 1$).

The index illustrates that the winds dominated the shelf circulation during both our summer and winter experiments, which are evidenced by vertical gray bars in Figure 16a. The situation is different, though, if we consider an entire year to estimate the forcing predominance. For $K = 11$ we found $|W_s| > 1$ near 48% of time, compared to 30% for

$K = 8$. This suggests that at least 30% of time the along-shelf circulation should be driven by winds, despite of the large plume of Rio de la Plata.

We also plot on Figure 16b a theoretical representation of the shelf currents, which we compute as sum of the buoyancy and wind-driven flows, $u_{shelf} = u_{wind} + u_{dis}$ for the average Kelvin number we found, $\bar{K} = 9$. The series suggests that downshelf (upshelf) circulations might occur 76% (24%) of the time. In the mean, $\bar{u}_{shelf} \approx +0.085$ m s^{-1} and downshelf, consistent with the residual northward coastal flow reported by Soares and Möller (2001) and Zavialov *et al.* (2002) from current meter observations to the north of our study area. We emphasize, however, that the theoretical arguments used here are an oversimplification of the shelf circulation. They assume, for example, that the structure of the plume is unaltered over time.

b. Across-shelf circulation history: Its importance to upwelling

The previous sections illustrated similarities of the along-shelf flow during summer and winter in response to upwelling-favorable winds. The response of the density field to those winds, however, was markedly different for the summer and winter surveys. We here explore the hypothesis that a fully developed upwelling event reflects both local winds as well as their history in time. Both control stratification and cross-shelf circulation.

Simplified models of upwelling circulation (Csanady, 1977; Cushman-Roisin, 1994) demonstrate that the efficiency of alongshore winds to drive a fully developed upwelling event depends on both the magnitude and the persistence of the winds, which is compactly expressed by a wind impulse integral over the wind event:

$$I = \int_{event} (\tau^y/\rho_o h)dt.$$

It is difficult to practically define an "event" so we follow Austin and Barth (2002) to introduce a formulation of the impulse integral with a decaying memory:

$$I_k(t) \approx \int_0^t (\tau^y/\rho_o h)e^{(t'-t)/k}dt'.$$

We estimated the above integral from alongshore winds, hence $I_k(t)$ represents a time integral of the Ekman transport perpendicular to the coastline. For instance, the across-shore Ekman transport can be obtained by multiplying I_k by h/f. This quantity can be estimated from a wind time series given the exponential time decay, k, in days. Results computed from Carrasco winds are shown on Figure 16c for $k = 3$ and 8 days, the typical synoptic interval of atmospheric disturbances in the region.

Results reflect a long-term pattern, where onshore transports preferentially occur between May and August and offshore transport occur between September and March. It

also becomes apparent that although weaker winds were blowing during the summer cruise, their cumulative effect upon surface water transport was substantial. Winter upwelling conditions during our survey were strong, but short especially relative to two strong and persistent onshore transport episodes just prior to our winter survey in August, which maintained the coastal plume structure by supporting strongly stratified waters prior to the onset of winds from the northeast.

The layered model proposed by Csanady (1977) allows a simple way to assess the possibility of a fully developed upwelling event as a function of stratification. His model predicts that the outcropping of the pycnocline should occur if the wind impulse integral surpasses a critical value $(g'h)^{1/2}$, which is dependent on the upper layer thickness and the water stratification $g' = g(\rho_2 - \rho_1)/\rho_2$ (ρ_1 and ρ_2 are the upper and lower layer densities). Here we plotted the observed typical summer ($\rho_1 = 1022$, $\rho_2 = 1024$ kg m^{-3}; per Fig. 13) and winter ($\rho_1 = 1017$, $\rho_2 = 1026$ kg m^{-3}; Fig. 13) critical values as horizontal bars centered along the observation period, along with $I_k(t)$ series on Figure 16c. We set $h = 15$ m for this analysis.

Because the observed vertical stratification was mild in the summer (horizontal bar in February, Fig. 16c), the weaker summer winds were sufficiently effective to promote a full upwelling that includes the outcropping of cold bottom waters at the surface. During our winter survey, however, neither the strength nor the duration of the wind event was able to generate enough impulse to overcome the high vertical stratification. Nevertheless, the year-long time series demonstrate that a few times winds were strong and persistent enough to overcome the strong vertical stratification associated with the Rio de la Plata plume, as observed in our winter survey. These events occurred in the Spring event of November 1999, Summer event of February 2000 and in the late Fall event of May of 2000.

c. *Monthly variability of cross-shelf transport*

In order to further inspect the long-term variability implied from the previous analysis, we analyzed winds derived from QuikSCAT (Level3b product), selecting the wind time series of 12 points situated along the Uruguayan coast (see squares on Fig. 17a). Our wind transport statistics was limited to the period of 1999–2007 covered by QuikSCAT observations.

We performed the computation of mean monthly wind vectors from these observations to illustrate the seasonal transition of the winds in this area, where easterly winds blow from late spring (October) to early fall (March) and southwesterlies are predominant for fall and winter (arrows on Fig. 17a). It is apparent how summer winds are nearly parallel to the coastline along Montevideo, Punta del Este (PDE) and Cape Polonio (CP).

In order to closely assess the effect of these winds blowing along the curved coastline of Uruguay (~480 km), we computed the Ekman transport $\tau_i/\rho f$ for each one of the selected QuikSCAT points, and evaluated the their total transport, $T(t)$, by

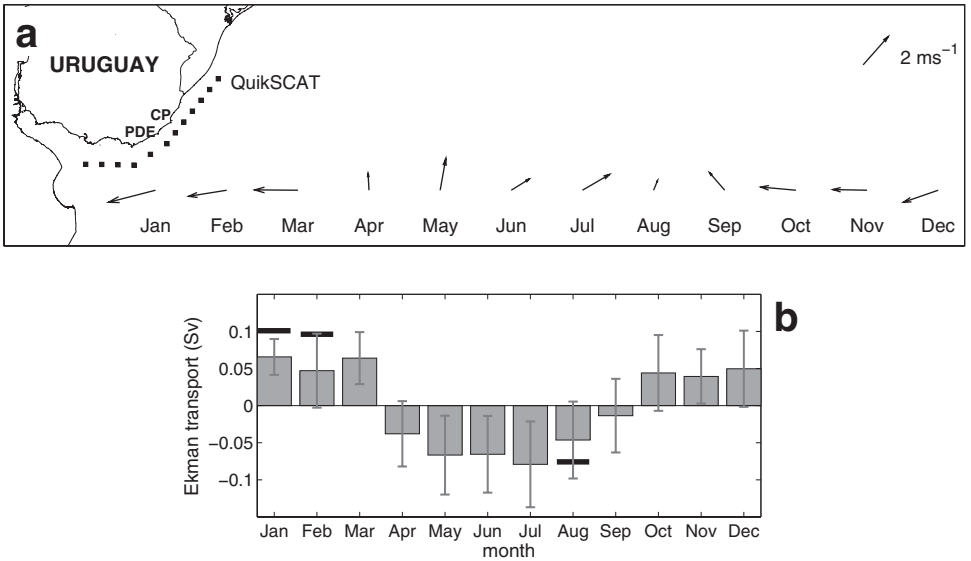

Figure 17. (a) Monthly wind vectors derived from QuikSCAT (1999–2007) coastal grid points, shown as small squares in the map. (b) Spatially integrated Ekman transport (1 Sv = 10^6 m^3 s^{-1}) derived from QuikSCAT winds (see text for details). Gray bars indicate monthly average transports along the entire coastal sector covered by the grid points of panel a. Positive (negative) values indicate offshore (onshore) transports. Vertical bars indicate ± 1 standard deviation of monthly averages and the thick horizontal bars are the monthly means for the RioPla cruises.

summing the contribution of each of the coastal segments cross-shore transports (Castelão and Barth, 2006):

$$T(t) = \sum_{i=1}^{N} \frac{\tau_i(t)}{\rho f}\, \delta s_i$$

Where τ_i is the wind component parallel to the i^{th} coastal segment of length δs_i (average length was 40 km). The result is displayed on Figure 17b in terms of monthly means of the total integrated transport.

The graph indicates the seasonal modulation of the winds, with offshore transport occurring preferably during the summer (Dec, Jan, Feb), including early spring (Oct., Nov.) and early fall (March). We note, however, that the standard deviation of the monthly transports (as shown by the vertical bars) was large, suggesting strong interannual variability. This means that the mean transport can reverse from what climatology suggests. For August 1999 (winter cruise) and for January and February of 2000 (summer cruises) we find monthly offshore transports nearly twice as large the computed means. The summer upwelling event covered, however, was of discrete magnitude if compared to the extension of the upwelling event of 1989 reported by Framiñan *et al.* (1999 Fig. 1). In

the winter, the mean transport was predominantly offshore but within the expected range of climatologic variability.

5. Summary and conclusions

Here we explored the elements of the dynamics of the coastal upwelling and shelf circulation off the coast of Uruguay in South America, a region influenced by large river discharges from the Rio de la Plata. Our findings indicate that despite the strong buoyancy forcing established by Plata, the subtidal along-shelf flow is largely modulated by winds. Winter observations describe a strong event of generally poleward currents that advect the buoyant plume upstream as a result of upwelling-favorable winds.

An analysis of a year-long wind strength index, a proxy of along-shelf circulation (Whitney and Garvine, 2005), showed that our winter upwelling observations were not an isolated event. Upwelling (poleward) circulation can occur at any time during the year. Along with Soares and Möller (2001), Zavialov *et al.* (2002) and Simionato *et al.* (2006) we demonstrate that the coastal currents off Uruguay and Southern Brazil are correlated with synoptic winds that frequently overcome the buoyancy forcing associated with the freshwater discharge from the Rio de la Plata.

Furthermore, the same winds that drive the along-shelf circulation also promote across-shelf exchange. The effect of upwelling-favorable winds over plumes is well described from models and observations (Fong and Geyer, 2001; Lentz and Largier, 2006). They cause coastal plumes to thin vertically, widen horizontally, and eventually separate from the coast as they move offshore. Observations from the Delaware coast (Münchow and Garvine, 1993a), the Gulf of Maine (Fong *et al.,* 1997) or the Columbia plume (Hickey *et al.,* 2005) show that an upwelling event is often capable to advect the surface plume offshore sometimes destroying its structure along the coast.

For the buoyant plume of the Rio de la Plata discharge, however, we showed that strong upwelling-favorable winds observed on winter did not destroy the plume. This behavior can be understood if we fairly compare the spatial scales of the Rio de la Plata plume to the scales of other plumes. With a typical offshore extension L $\approx$100 km and depth of h $\approx$ 50 m, the Rio de la Plata plume has a triangular cross-sectional area of about $A_{Plata} \approx Lh/2 \approx 2.5$ km^2. This figure, for instance, is nearly 16 times the cross-sectional area of the Delaware plume (L $\approx$ 20 km; h $\approx$15 m, $A_{Del} \sim 0.15$ km^2; Münchow and Garvine, 1993b). Therefore, it seems unlikely that a single wind event should severely alter the more robust Plata cross-shelf structure.

From this consideration, we can establish a simple argument that helps to classify the different behavior of large-scale coastal plumes to upwelling events. The argument involves the comparison of two time scales. The first is of advective nature, namely $t_{adv} \approx A/(\tau/\rho f)$, where A represents a buoyant plume cross-sectional area and $\tau/\rho f$ is the cross-shelf Ekman flux (m^2 s^{-1}). This represents the typical time taken to completely export buoyant plume waters offshore. The second time scale is the wind event scale, t_e.

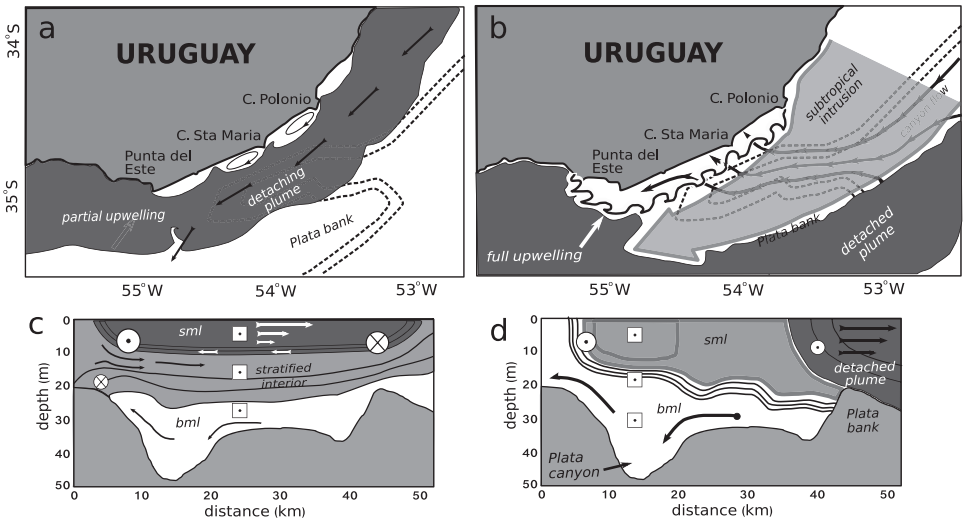

Figure 18. Schematic illustrating data-derived characteristic of the upwelling circulation observed for the Uruguayan shelf in a horizontal (a and b) and vertical (c and d) plane. In (a) and (c) winds reverse the along-shelf circulation ($Ws < -1$), but the upwelling is inefficient ($\Gamma < 1$) so the plume is partially detached from the coast keeping highly stratified nearshore waters (S > 0.45, where $S \approx N\alpha/f$ is the Burger number). In (b) and (d), besides the poleward circulation ($Ws < -1$), wind events promote the complete detachment of the plume ($\Gamma \geq 1$), reducing the nearshore stratification (S ~ 0.14), promoting cold water upwelling and the intrusion of subtropical waters.

Their ratio forms a dimensionless parameter $\Gamma \equiv t_e/t_{adv}$ that we call "upwelling age" and which expresses the efficiency of a wind event to alter a plume structure.

We expect that an upwelling-favorable wind stress of $\tau \approx 0.1$ Nm^{-2}, would significantly alter the structure of the Delaware plume within $t_{adv} \approx 1.6$ days, while for the Rio de la Plata plume the same response would require at least 24 days. Hence the Delaware plume is sensitive ($\Gamma \geq 1$) to typical wind events ($t_e \approx 3$ days) while the Rio de la Plata plume is not ($\Gamma \ll 1$). This argument can also explain the observed seasonal response to upwelling-favorable winds. In the winter, frequent downwelling winds return the Rio de la Plata plume water toward the coast, thus restoring its structure. Therefore, the time-integrated upwelling efficiency is often weak despite of the strong upwelling-favorable winds and upshelf circulation (Fig. 18a). In the summer, however, major downwelling events are rare, and the cumulative effect of a sequence of weak upwelling winds detaches the Rio de la Plata from the coast. The upwelling age is clearly $\Gamma \geq 1$ in this case (Fig. 18b).

An important consequence of this cumulative cross-shelf exchange is the modification of the vertical stability of Uruguayan waters. During the winter, the partially detached plume imposes strongly stratified coastal waters. The velocity and temperature fields indicate that convergence of nearshore waters along the inner-shelf front promotes sinking

through the thick stratified interior layers (Fig. 18c), as indicated by vertical temperature inversions. These inversions are distinct from those observed by Castello and Möller (1977) in south Brazil where the thermocline is established by the presence of warm tropical waters offshore associated with the Brazil Current. In the summer the shelf is less stratified than in winter because the plume waters are exported offshore. This increases the likelihood of cold water to outcrop at the surface and allows the development of thick surface and bottom mixed layers flowing in opposite directions (Fig. 18d).

The coastal upwelling ultimately relates to the bottom morphology of the Uruguayan shelf, as the Rio de la Plata canyon acts as a conduit of cold and deep shelf waters. These waters flow through the canyon and contribute to the cold surface signature of the surface waters (Fig. 18d). As the canyon is shallow ($h_{canyon} \sim 60$ m) the bottom flow field is characterized by larger Ekman numbers ($E_K \approx \delta_{ek}/h_{canyon} \sim 0.5$ to 1) in comparison to deeper shelfbreak canyons ($E_K \approx 0.05$), which suggests that bottom Ekman layers should play an important role in the circulation. The mechanism of exchange through the canyon is particularly important, because we find Rio de la Plata plume waters mixed with ambient shelf waters close to the bottom offshore and above the Rio de la Plata bank. This submarine bank forms an offshore ridge that blocks the advection of upwelled waters from the shelfbreak (Fig. 18d).

We found along-shelf currents coherent to the summer and winter density fields. The thermal wind balance explained vertical velocity shear well, even in waters as shallow as 20 m or in the summer, when a continuously stratified interior layer was much diminished. The summer upwelling region was associated with a poleward jet nearshore, but it also contained a weak poleward flow that was driven by cross-shore density gradients associated with the Rio de la Plata plume waters (Fig. 18d). In winter, the plume configuration caused strong cross-shelf shear of along-shelf currents (Fig. 18c).

Our analysis reveal that despite the large buoyant outflow from the Rio de la Plata River, the coastal upwelling should display a seasonal character, being related to variations of the South Atlantic high pressure system. During the spring and summer months, the predominant northeasterly winds progressively act to export Rio de la Plata plume waters offshore, thus reducing the shelf stratification and increasing the chances of a full upwelling. The occurrence of upwelling during the winter season is interrupted by strong downwelling events, which tends to advect Rio de la Plata buoyant waters northward and back toward the shore, "capping" the upwelling center. Despite the implied seasonal signal, the interannual variability of Ekman transport in this region was significant, possibly leading to the extreme promotion (or suppression) of Uruguay upwelling system.

Acknowledgments. This project was part of a collaborative effort between US universities and the Naval Hydrographic Service (SHN) from the Argentine Navy, funded by NSF International Programs as a supplement to OCE (9529806). The first author acknowledges the Brazilian CAPES foundation for his support (BEX 2242/03-6) at the University of Delaware. Partial support was also provided by the Mary A. S. Lighthipe Endowment to the University of Delaware. We are grateful to Mariana Framiñan, Arnoldo Valle-Levinson and the crew of B.H.A.R.A. "Comodoro Rivadavia" for their enthusiasm in the oceanographic surveys. We are also thankful to Dong Ping Wang and Richard

Table 1. Source of parameters used in the plume Kelvin number computation.

Source	Location	Season	Temperature/salinity Plume	Ambient	$L(km)$	$h_p(m)$	$R_{di} = \sqrt{g' h_p}/f$	$K = L/R_{di}$
Soares and Möller (2001)	Albardão, 33S	Fall	15°C/30	17°C/34	125–150	50–60	14.45 km	9.52
″	Albardão, 33S	Spring	13°C/30	14°C/34	100–150	40–50	13.71 km	9.12
″	Albardão, 33S	Winter	13°C/31	14°C/34	100–140	50	12.37 km	9.7
Möller *et al.* (2008)	Rio Grande, 32S	Winter	13°C/30	17°C/34	150	60	13.89 km	10.8
″	P. del Diablo, 34S	Winter	11°C/30	14°C/34	115	60	14.8 km	7.77
Piola *et al.* (2008)	Albardão, 33S	Winter	11°C/30	14°C/34	120	60	14.8 km	8.11
							$\bar{R}_{di} = 14.0$	$\bar{K} = 9.17$

Pawlowicz for providing the software to process the ADCP data. We thank Carlos Martinez and the Servício de Oceanografía, Hidrografía y Meteorología de la Armada Uruguaya (SOHMA) the Meteorology Laboratory of the University of Rio Grande (FURG) and the Subsecretaría de Recursos Hídricos of Argentina for respectively providing sea level, meteorological buoy and stream flow data. NCEP Reanalysis data were provided by the NOAA/OAR/ESRL PSD, Boulder, Colorado, USA, from their site at http://www.cdc.noaa.gov/ and QuikSCAT wind fields by NASA Jet Propulsion Laboratory at http://podaac.jpl.nasa.gov. Meteorological tower data is due to National Climate Data Center (NESDIS/NOAA) at http://www.ncdc.noaa.gov/oa/ncdc.html. We are grateful for the critical review of this research provided by A. D. Kirwan, Jr., Patricia Eichler and two anonymous reviewers. Figure 1 is Copyright 1999, Springer Publishing reprinted with permission. This paper is dedicated to the memory of Prof. Richard Garvine and gratefully acknowledges his patient mentoring, continuing inspiration and many enlightening contributions to the field of physical oceanography.

APPENDIX

The evaluation of the theoretical discharge velocity, u_{dis}, of Whitney and Garvine (2005) involve the plume Kelvin number, a parameter that scales the plume width to the internal Rossby radius of deformation. Here we computed the Kelvin number from different hydrographic transects of Plata plume published in the scientific literature. The sources of data, thermohaline properties of the plume and ambient waters, as well as the estimated Kelvin numbers are indicated on Table 1. Note that L is the cross-shelf distance of Plata plume measured on surface in reference to the isohaline of ~33.5, which is suggested as the limit of plume waters (Möller *et al.,* 2008). The parameter h_p is defined as the maximum depth, or the depth of the foot of the plume. Available summer observations of Plata plume demonstrated substantial change due to winds, so we do not include it in this estimation.

REFERENCES

Acha, E. M., H. W. Mianzan, R. A. Guerrero, M. Favero and J. Bava. 2004. Marine fronts at the continental shelves of austral South America. Physical and ecological process. J. Mar. Sys., *44,* 83–105, doi:10.1016/j.jmarsys.2003.09.005.

Austin, J. A. and J. A. Barth. 2002. Variation in the position of the upwelling front on the Oregon shelf. J. Geophys. Res., *107,* 3180, doi:10.1029/2001JC000858.

Bakun, A. 1996. Patterns in the Ocean. Ocean Process and Marine Population Dynamics, California Sea Grant (NOAA) and Centro de Investigaciones Biológicas del Noroeste, La Paz, México, 323 pp.

Berbery, E. H. and V. R. Barros. 2002. The hydrologic cycle of the La Plata basin in South America. J. Hydrom., *3,* 630–645.

Brainerd, K. E. and M. C. Gregg. 1995. Surfaced mixed and mixing layer depths. Deep-Sea Res. I, *42,* 1521–1543.

Bretherton, F. P., R. E. Davis and C. B. Faundry. 1976. A technique for objective analysis and design of oceanographic experiments applied to MODE-73. Deep-Sea Res., *23,* 559–582.

Candela, J., R. C. Beardsley and R. Limeburner. 1992. Separation of tidal and subtidal currents in ship-mounted acoustic doppler current profiler observations. J. Geophys. Res., *97,* 769–788.

Castelão, R. M. and J. A. Barth. 2006. Upwelling around Cabo Frio, Brazil: The importance of wind stress curl, Geophys. Res. Lett., *33,* L03602, doi:10.1029/2005GL025182.

Castello, J. P. and O. M. Möller. 1977. Sobre as condições oceanográficas no Rio Grande do Sul. Rev. Atlântica, *2,* 25–110.

Castro, B. M. and L. B. Miranda. 1998. Physical oceanography of the western Atlantic continental shelf between 4° N and 34° S, *in* The Sea-Global Coastal Oceans,*10,* K. Brink and A. Robinson eds., John Wiley and Sons, 209–251.

Clarke, A. J. and D. S. Battisti. 1981. The effect of continental shelves on tides. Deep-Sea Res. Part A. Oceanog. Res. Pap., *28,* 665–682, doi:10.1016/0198-0149(81)90128-X.

Csanady, G. T. 1977. Intermittent full upwelling in Lake Ontario. J. Geophys. Res., *82,* 397–419.

Cushman-Roisin, B. 1994. Introduction to Geophysical Fluid Dynamics, Prentice Hall, 320 pp.

Dragani, W. C., C. G. Simionato and M. N. Nunez. 2002. About the vertical structure of currents in the intermediate Rio de la Plata. Observational study. Geoacta, *27,* 71–84.

Ebuchi, N., H. C. Graber and M. J. Caruso. 2002. Evaluation of wind vectors observed by QuikSCAT/SeaWinds using ocean buoy data. J. Atmos. Oceanic Technol., *19,* 2049–2062.

Emery, W. J. and R. E. Thomson. 1997. Data Analysis Methods in Physical Oceanography, Elsevier, 638 pp.

Emilson, I. 1960. The shelf and coastal waters off southern Brazil. Bol. Inst. Oceanog. USP, *144,* 101–111.

Fong, D. A. and W. R. Geyer. 2001. Response of a river plume during an upwelling-favorable wind event. J. Geophys. Res., *106,* 1067–1084.

Fong, D. A., W. R. Geyer and R. P. Signell. 1997. The wind-forced response on a buoyant coastal current: Observations of the western Gulf of Maine plume. J. Mar. Syst., *12,* 69–81.

Foreman M. G. G. and H. J. Freeland. 1991. Comparison of techniques for tide removal from ship-mounted acoustic Doppler measurements along the southwest coast of Vancouver Island. J. Geophys. Res., *96,* 17007–17021.

Framiñan, M. B. 2005. On the physics, circulation and exchange process of the Rio de la Plata estuary and adjacent shelf. Ph.D. thesis, University of Miami, Coral Gables, Florida, USA, 486 pp.

Framiñan, M. B., M. P. Etala, E. M. Acha, R. A. Guerrero, C. A. Lasta and O. B. Brown. 1999. Physical characteristics and process of the Rio de la Plata estuary, *in* Estuaries of South America: Their Geomorphology and Dynamics, G. M. E. Perillo, M. C. Piccolo and M. P. Quivira, eds., Springer Verlag, 161–194.

Freeland, H. J. and K. L. Denman. 1982. A topographically controlled upwelling center off southern Vancouver Island. J. Mar. Res., *40,* 1069–1093.

Gan, M. A. and V. B. Rao. 1991. Surface cyclogenesis over South America. Mon. Weather Rev., *119,* 1293–1302.

Garvine, R. W. 2004. The vertical structure and subtidal dynamics of the inner shelf off New Jersey. J. Mar. Res., *62,* 337–371.

Guerrero, R. A., E. M. Acha, M. B. Framiñan and C. A. Lasta. 1997. Physical oceanography of the Rio de la Plata estuary, Argentina. Cont. Shelf Res., *17,* 727–742.

Hickey, B. M. 1997. The response of a steep-sided, narrow canyon to time-variable wind forcing. J. Phys. Oceanogr., *27,* 697–726.

Hickey, B. M., S. Geier, N. Kachel and A. MacFadyen. 2005. A bi-directional river plume: the Columbia in summer. Cont. Shelf Res., *25,* 1631–1656.

Hill, A. E., B. M. Hickey, F. A. Shillington, P. T. Strub, K. Brink, E. D. Barton and A. C. Thomas. 1998. Eastern ocean boundaries. Coastal segment (E), *in* The Sea-Global Coastal Oceans, K. Brink and A. Robinson, eds., John Wiley and Sons, Inc., 29–67.

Huyer, A., J. H. Fleischbein, J. Keister, M. P. Kosro, N. Perlin, R. L. Smith and P. A. Wheeler. 2005. Two coastal upwelling domains in the northern California Current system. J. Mar. Res., *63,* 901–929.

Joyce, T. M. 1989. On *in situ* "calibration" of shipboards ADCPs. J. Atmos. Oceanic Technol., *6,* 169–172.

Kalnay, E., M. Kanamitsu, R. Kistler, W. Collins, D. Deaven, L. Gandin, M. Iredell, S. Saha, G. White, J. Woollen, Y. Zhu, A. Leetmaa, B. Reynolds, M. Chelliah, W. Ebisuzaki, W. Higgins, J. Janowiak, K. Mo, C. Ropelewski, J. Wang, R. Jenne, and D. Joseph. 1996. The NCEP/NCAR 40-Year Reanalysis Project. Bull. Amer. Meteor. Soc., *77,* 437–471.

Kämpf, J. 2006. Transient wind-driven upwelling in a submarine canyon: a process-oriented modeling study, J. Geophys. Res., *111,* doi:10.1029/2006JC003497.

Klinck, J. M. 1996. Circulation near submarine canyons: a modeling study. J. Geophys. Res., *101,* 1211–1223.

Laborde, J. P. and G. J. Nagy. 1999. Hydrography and sediment transport characteristics of the Rio de la Plata: a review, *in* Estuaries of South America: Their Geomorphology and Dynamics, G. M. E. Perillo, M. C. Piccolo and M. P. Quivira, eds., Springer Verlag, 134–159.

Large, W. G. and S. Pond. 1981. Open ocean momentum flux measurements in moderate to strong winds. J. Phys. Oceanogr., *11,* 324–336.

Lentz, S. J. 1992. The surface boundary layer in coastal upwelling regions. J. Phys. Oceanogr., *22,* 1517–1539.

Lentz, S. J. and J. Largier. 2006. The influence of wind forcing on the Chesapeake Bay buoyant coastal current. J. Phys. Oceanogr., *36,* 1305–1316.

Miranda, L. B. 1972. Propriedades e variáveis físicas das águas da plataforma continental do Rio Grande do Sul. Ph.D. thesis, Instituto Oceanográfico da Universidade de São Paulo, Praça do Oceanográfico, 191, Cid. Universitária.—São Paulo—SP–Brazil, 127 pp.

Möller, O. O., A. R. Piola and A. C. Freitas. 2008. The effects of river discharge and seasonal winds on the shelf off southeastern South America. Cont. Shelf Res., doi:10.1016/j.csr.2008.03.012.

Münchow, A., C. S. Coughran, M. C. Hendershott and C. D. Winant. 1995. Performance and calibration of an acoustic doppler current profiler towed below the surface. J. Atmos. Oceanic Technol., *12,* 435–443.

Münchow, A. and M. B. Framiñan. 2000. Wind buoyancy and topographic forcing in the Rio de la Plata region of freshwater influence near 35S latitude. EOS Trans., AGU, *81,* OS165.

—— 2001. Kinematics of a topographically steered poleward shelf flow off Uruguay. Proceedings of the Joint IAPSO/IABO Assembly, Mar del Plata, Argentina, IB01-96.

Münchow, A. and R. W. Garvine. 1993a. Buoyancy and wind forcing of a coastal current. J. Mar. Res., *51,* 293–322.

—— 1993b. Dynamical properties of buoyancy–driven coastal current. J. Geophys. Res., *98,* 20063–20077.

Olson, D., G. Podesta, R. Evans and O. Brown. 1998. Temporal variations in the separation of the Brazil and Malvinas currents. Deep-Sea Res., *35,* 1971–1990.

Palma, E. D., R. P. Matano and A. R. Piola. 2004. A numerical study of the Southwestern Atlantic shelf circulation: barotropic response to tidal and wind forcing. J. Geophys. Res., *109,* C08014, doi:10.1029/2004JC002315.

Pawlowicz, R., B. Beardsley and S. Lentz. 2002. Classical tidal harmonic analysis including error estimates in MATLAB using T_TIDE. Comp. Geosci., *28,* 929–937.

Pereira, C. S. 1989. Seasonal variability in the coastal circulation on the Brazilian continental shelf (29S–35S). Cont. Shelf Res., *9,* 285–299.

Pickett, M. H., W. Tang, L. K. Rosenfeld and C. H. Wash. 2003. QuikSCAT satellite comparisons with nearshore buoy wind data off US west coast. J. Atmos. Oceanic Technol., *20,* 1869–1879.

Piola, A. R., E. J. D. Campos, O. O. Möller, M. Charo and C. Martinez. 2000. Subtropical shelf front off eastern South America. J. Geophys. Res., *105,* 6565–6578.

Piola, A. R., O. O. Möller, R. A. Guerrero, E. J. D. Campos. 2008. Variability of the subtropical shelf front off eastern South America: Winter 2003 and summer 2004. Cont. Shelf Res., doi:10.1016/j.csr.2008.03.013.

RD Instruments. 1996. Acoustic Doppler Current Profiler. Principles of Operation: A Practical Primer. Tech. report, San Diego, California, 52 pp.

Sepulveda, H. H., A. Valle-Levinson and M. B. Framiñan. 2004. Observations of subtidal and tidal flow in the Rio de la Plata estuary. Cont. Shelf Res., *24,* 509–525.

She, J. and J. M. Klinck. 2000. Flow near submarine canyons driven by constant winds. J. Geophys. Res., *105,* 28671–28694.

Silveira, I. C. A., A. C. K. Schmidt, E. J. D. Campos, S. S. Godoi and Y. Ikeda. 2000. A corrente do Brasil ao largo da costa leste brasileira. Braz. J. Oceanogr., *48,* 171–183.

Simionato, C. G., V. L. Meccia, W. C. Dragani, R. Guerrero, and M. Nuñez. 2006. Rio de la Plata estuary response to wind variability in synoptic to intraseasonal scales: barotropic response. J. Geophys. Res., *111,* doi:10.1029/2005JC003297.

Simionato, C. G., V. Meccia, W. Dragani and M. Nunez. 2005. Barotropic tide and baroclinic waves observations in the Rio de la Plata estuary. J. Geophys. Res., *110,* doi:10.1029/2004JC002842.

Smith, R. L. 1994. The physical process of coastal ocean upwelling systems, *in* Upwelling in the Ocean: Modern Process and Ancient Records, C. P. Summerhayes *et al.,* eds., John Wiley and Sons, 422 pp.

Soares, I. D. and O. O. Möller. 2001. Low-frequency currents and water mass spatial distribution on the southern Brazilian shelf. Cont. Shelf Res., *21,* 1785–1814.

Stramma, L. and M. England. 1999. On the water masses and mean circulation of the South Atlantic ocean. J. Geophys. Res., *104,* 20863–20883.

Summerhayes, C. P., K. C-. Emeis, M. V. Angel, R. L. Smith and B. Zeitzschel. 1994. Upwelling in the Ocean: Modern Process and Ancient Records, *in* Upwelling in the Ocean: Modern Process and Ancient Records, C. P. Summerhayes *et al.,* eds., John Wiley and Sons, 422 pp.

Vivier, F. and C. Provost. 1999. Direct velocity measurements in the Malvinas Current. J. Geophys. Res., *104,* 21083–21103.

Wang, D. P. 2007. Spatial Data Analysis Using Matlab, Marine Sciences Research Center, State University of New York Stony Brook, 27 pp.

Wang, Y. H., S. Jan and D. P. Wang. 2003. Transports and tidal current estimates in the Taiwan Strait from shipboard ADCP observations (1999–2001). Estuar. Coast. Shelf Sci., *57,* 193–199.

Whitney, M. M. and R. W. Garvine. 2005. Wind influence on a coastal buoyant outflow. J. Geophys. Res., *110,* doi:10.1029/2003JC002261.

Yankovsky, A. E., R. W. Garvine and A. Münchow. 2000. Mesoscale currents on the inner New Jersey shelf driven by the interaction of buoyancy and wind forcing. J. Phys. Oceanogr., *30,* 2214–2230.

Zavialov, P. O., O. O. Möller and E. J. D. Campos. 2002. First direct measurements of currents on the continental shelf of southern Brazil. Cont. Shelf Res., *22,* 1975–1986.

Received: *4 December, 2007;* revised: *5 August, 2008.*